THE JOHNS HOPKINS UNIVERSITY
APPLIED PHYSICS LABORATORY
SILVER SPRING, MARYLAND

OPTICAL INVESTIGATIONS OF NON-CRYSTALLINE SEMICONDUCTORS

FINAL TECHNICAL REPORT

Covering the period February 1, 1970 to January 31, 1973

NASA Grant #NGR 21-009-033

Prepared by:

N. A. Blum
C. Feldman
K. Moorjani

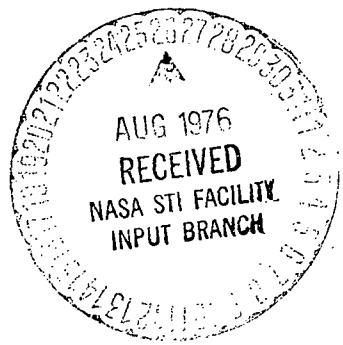

INTRODUCTION

This final technical report describes the results of work performed at this Laboratory under NASA Grant No. NGR-009-033. This Grant was one of the earliest Government supported research projects in the area of amorphous semiconductors. Until recently, solid state physics had been concerned primarily with crystalline materials - a concern which has led to a revolution in electronics technology. The study of the fundamental properties of disordered semiconductors indicates that many of these properties responsible for the huge technological success of crystalline materials are still present in the disordered materials. In addition, the disordered systems hold much promise for contributing their own unique attributes to the development of semiconductor technology. For example, their insensitivity to structural changes, wrought by exposure to hostile ambient conditions such as temperature fluctuations and radiation fields, immediately suggests their application to certain classes of hardened devices. But, as in the case of crystalline semiconductor technology, the fundamental physical properites, materials characterization and basic theory must establish a firm foundation before there can be much chance of significant technological advance.

During the two years covered by this report, we have investigated the optical properties of carefully prepared amorphous silicon and boron. Much has been learned about characterizing these materials and measuring their purities. The groundwork has been prepared for understanding the behavior and properties of amorphous semiconductors and for the fabrication of useful devices based upon such an understanding. A number of technical reports have appeared in the scientific

literature (see Appendix listing 6 references published with NASA support) and a paper on the optical properties of amorphous silicon and boron films is being prepared. Our work on disordered semiconductors has developed a firm foundation under NASA sponsorship and further work is being continued under alternate sponsorship.

This report covers three areas of investigation into the properties of non-crystalline materials: (1) optical properties of elemental amorphous semiconductors, (2) Mössbauer studies of disordered systems, and (3) theoretical aspects of disordered semiconductors. These will be described briefly below. Background material has been provided in the original proposal [1]. Detailed results of the completed work have been, or will soon be, published. The detailed results which have been published are attached to this report.

Optical Properties of Elemental Amorphous Semiconductors

Optical absorption studies of solids are a classic means of determining fundamental properties of semiconductors such as band gaps, density of states, and impurity levels. Optical studies have, of course, accompanied and aided the development of crystalline semiconducting devices. In the investigation of amorphous materials, optical studies are playing a similar role, but a great deal of controversy surrounds the interpretation of the results. The sharpness of the band edge, for example, is still not entirely resolved. Some investigators have observed sharp band edges in amorphous germanium and silicon, while others have observed tails. Band tailing is expected according to the presently accepted theory of disordered systems.

Optical studies in amorphous materials are somewhat more difficult than similar studies on crystalline systems. The samples investigated in this report are in the form of thin films. There are problems associated with sample purity during fabrication, substrate influence, optical interference effects, and surface contamination after the sample is removed from the vacuum. Exploring the band tails in amorphous systems also requires greater sensitivity and lower background than is usually employed for normal crystal studies.

An optical apparatus was constructed to maintain the sample purity and provide the sensitivity necessary to explore the spectral absorption of amorphous materials. The optical facility developed under the NASA Grant includes a double-beam spectrometer for recording transmission spectra over a wide range of sample environments. The instrument is extremely versatile in that almost any combination of energy sources, gratings, and detectors may be used to obtain spectra over the range from 2000 A in the ultra-violet to 4μ in the near infra-red. The novel electronic detection scheme allows accurate transmittance measurements to be made down to 0.1% of the reference signal, while the SPEX Model 1400-11 double grating spectrometer provides excellent spectral accuracy and high resolution.

The complex refractive index for each sample was determined by a computer analysis of the transmission versus wavelength data for a pair of similarly prepared thin films of different thicknesses. A computer program was developed which properly takes into account the multiple reflections between the thin amorphous film and the air as well as those reflections between the substrate of known refractive index (usually quartz) and the film on one side and air on the other. Transmission data for two films identically prepared except for thickness are analyzed to give the index of refraction n and the absorption coefficient α for the amorphous film.

Preliminary results for silicon (Appendix I) and boron films (Appendix II) have been presented at appropriate technical symposia. A comprehensive summary of our findings is being prepared for publication in a technical journal with copies to be sent to NASA as an addendum to this report. Figure 1 shows the variation with photon energy of the refractive index n and the absorption coefficient α for similarly prepared amorphous and crystalline silicon films. These data clearly show the presence of an absorptive tail in the amorphous films and the absence of such a tail in the crystalline films.

The process of crystallization of amorphous films is not well understood. We have investigated the crystallization process in amorphous silicon films by observing optical transmission changes in the films as they are heated at various temperatures for different lengths of time. A model for describing crystallization process was formulated and the silicon film data fitted to the model. We believe the result to be applicable to other systems as well as silicon. A detailed report appears in the literature (see Appendix III).

In connection with the optical investigations sponsored by NASA, we have for some time been concerned with the preparation and analysis of ultra pure silicon films. The technique of sputter-ion source mass analysis of the films has been used to characterize the purity of the films and as an aid in obtaining purer films. The technique is also useful in determining bonding and clustering of atomic neighbors in the films. This work has been described in earlier Progress Memoranda to NASA [2]. A more detailed account of this work, which was not supported by the NASA Grant, has been published elsewhere [3]. The ultra pure samples were, of course, used in the NASA optical study.

Mössbauer Studies of Disordered Systems

The Mössbauer technique has been established as a useful method for investigating the microscopic structure of matter. Its application to the study of disordered solids is outlined in the proposal [1].

Under NASA sponsorship, the experimental apparatus was acquired and tested. Efforts were made to design a system for investigating amorphous tellurium films by Mössbauer spectroscopy. The NASA program was terminated before any satisfactory amorphous tellurium films could be obtained.

Recently we have, however, succeeded in preparing amorphous tellurium films which give good Mössbauer spectra. There are dramatic differences between the spectra of the amorphous and crystallized samples. The experimental work and its interpretation are continuing at this Laboratory under alternate sponsorship (AROD). Preliminary results indicate that, as we anticpated, the Mössbauer technique is extremely sensitive to changes in the structure of films.

Theoretical Aspects of Disordered Solids

Theoretical work, in collaboration with scientists from other institutions, has centered on the extension of the single-site Coherent Potential Approximation to include the effects of scattering from pairs of sites and off-diagonal randomness. Both weak and strong scattering cases have been analyzed. The numerical results for the density of states have been obtained for various disordered binary alloys. Detailed results have been published and are included in Appendices IV, V and VI. The model has also been applied to investigate the effect of magnetic disorder on the spin wave spectrum and the curie temperature of a randomly disordered spin-$\frac{1}{2}$ Heisenberg ferromagnet. In addition, computer programs for analyzing optical transmission data were developed and modified for interpreting the experiments performed on silicon and boron films.

REFERENCES

(1) "Proposal for Optical and Mössbauer Investigations of Non-Crystalline Materials", Document #AD-4885, The Johns Hopkins University, Applied Physics Laboratory, October 9, 1970.

(2) "Progress Memoranda", The Johns Hopkins University, Applied Physics Laboratory, PEG-002 (May 28, 1971) and PEG-003 (January 17, 1972) under NASA Grant No. NGR 21-009-033, Supplement #1.

(3) "The Study of Amorphous and Crystalline Silicon Thin Films by Sputter-Ion Source Mass Spectroscopy", C. Feldman and F. G . Satkiewicz, Thin Solid Films 12, 217 (1972) and "Mass Spectra Analyses of Impurities and Ion Clusters in Amorphous and Crystalline Silicon Films", C. Feldman and F. G. Satkiewicz, J. Electrochemical Soc., (to be published in August 1973).

APPENDIX

Papers Published Citing Support under NASA Grant No. NGR 21-009-033

I. "Optical Properties of Amorphous Silicon Films, N. A. Blum, C. Feldman and K. Moorjani, Bull. Am. Phys. Soc. 17, 114 (1972).

II. "Mass Spectrometry, Optical Absorption and Electrical Properties of Amorphous Boron Films", C. Feldman, K. Moorjani and N. A. Blum, Proc. Intl. Symposium on Boron, 1973 (to be published).

III. "The Crystallization of Amorphous Silicon Films", N. A. Blum and C. Feldman, J. Non-Crystalline Solids 11, 242 (1972).

IV. "Pair Approximation in the Coherent Potential Theory of Off-Diagonal Randomness", K. Moorjani, T. Tanaka and S. M. Bose, Conduction in Low-Mobility Materials, Ed. N. Klein, D. S. Tannhauser and M. Pollak (Taylor and Francis Ltd., London 1971), pp. 167-173.

V. "Coherent Potential Theory of Off-Diagonal Randomness: Binary Alloy", T. Tanaka, M. M. Sokoloski, K. Moorjani and S. M. Bose, J. Non-Crystalline Solids 8-10 155 (1972)

VI. "Coherent Potential Theory of a Random Binary Alloy: Effects of Scattering from Two-Sites Clusters and Off-Diagonal Randomness", K. Moorjani, T. Tanaka, M. M. Sokoloski and S. M. Bose (submitted for publication).

Abstract submitted for the Annual Meeting of
The American Physical Society, January 31-February 3, 1972

Published in Bull. Am. Phys. Soc. 17, 114 (1972)

Optical Properties of Amorphous Silicon Films.* N. A. BLUM, C. FELDMAN and K. MOORJANI, Applied Physics Lab. The Johns Hopkins U.--
Amorphous films (~ .5 to 1.0 mμ thick) of well characterized pure Si were prepared by vacuum deposition on fused silica substrates under carefully controlled conditions. Sputter-ion mass spectrometry has provided information concerning the purity and composition of the films. Optical transmission studies on films of various thicknesses has yielded values for the complex refractive index over the wavelength range 0.4 to 2.5 mμ. The absorption spectra clearly show the presence of an absorptive tail at the longer wavelengths relative to identically prepared films which were subsequently crystallized. The results will be discussed in terms of recent models affecting the tailing of the density of states in amorphous materials. A double beam spectrophotometer has been designed for these experiments and will be described briefly.

*Work supported in part by NASA Grant No. NGR 21-009-033.

APPENDIX II

Mass Spectrometry, Optical Absorption and Electrical Properties of Amorphous Boron Films*

Charles Feldman, Kishin Moorjani and Norman Blum
Applied Physics Laboratory - The Johns Hopkins University
8621 Georgia Avenue, Silver Spring, Maryland 20910

ABSTRACT

Electrical conduction and optical absorption in pure films of amorphous boron are described. Sputter-ion source mass spectrometry was used to investigate the purity of the films and showed that the previous samples, deposited from graphite crucibles, contained a large amount of carbon. Various sources of impurities during vacuum deposition were identified. The sputter-ion source mass spectrometry also gives information about the boron ion-clusters ejected from these films. The cluster spectra shows peaks at B_5^+, suggesting a coordination number of 5 for amorphous films. The temperature dependence of electrical resistivity identifies activation energies at 0.14 eV, 0.35 eV and 0.65 eV. The optical absorption edge in amorphous boron is considerably broadened and shifted toward lower energies as compared to the crystalline case. The absorption coefficient α, for values $\geq 10^4$ cm^{-1}, follows the expression $(h\nu - E_g)^2/h\nu$ and for lower values can be fitted to an exponential $e^{h\nu/E_a}$. The values of the parameters E_a and E_g are determined to be 0.12 eV and 0.62 eV respectively. These results are discussed and compared with those reported in the literature.

* Supported by Naval Ordnance Systems Command
Contract N00017-72-C4401, Task A13B

I. Introduction

Efforts since the previous Boron Conference have been concentrated on the improvement and refinement of techniques for producing thin films. Refinements have been made in vacuum techniques for producing the films and in optical techniques for measuring their optical properties. A sputter-ion source mass spectrometer has been used to analyze the films from the standpoint of purity and ion clusters, and this information has been used to improve the purity of the films. The methods for producing purer films and the conditions during vacuum deposition are described in the next section. The purity of these samples as determined by sputter-ion source mass analysis is discussed in Section III. It is found that the films described in previous reports contain large amounts of carbon. Section IV deals with the analysis of boron ion clusters in amorphous films as well as in the bulk material. The electrical conduction and the optical absorption in the purer samples are discussed and compared with earlier results in Sections V and VI respectively. Finally, the last section contains some concluding remarks on the present findings.

II. Film Preparation

Samples were deposited in a 12" water-cooled stainless steel vacuum bell jar. The system was evacuated by means of a mechanical pump, an oil diffusion pump and a titanium getter pump. Appropriate zeolite and liquid nitrogen traps are included in the system. The

pre-deposition pressure was less than 5×10^{-9} torr. Deposition pressures were between 7×10^{-8} and 1×10^{-7} torr. The deposition parameters for the samples described here are given in Table I. Sample B-44 was deposited in a carbon crucible at a pressure of 2×10^{-6} in a similar manner to that described in the previous Conference [1]. An analysis of this film, to be discussed later, showed that it contained a large quantity of carbon. Sample B-66 was deposited from a silver-plated copper, water-cooled crucible, and Sample B-62 and subsequent films used water-cooled stainless steel crucibles with molybdenum liners. A photograph of this crucible and arrangement in the system is shown in Fig. 1. The large diameter (3.5 cm) of the source allowed one to obtain a fast deposition rate. The elimination of the carbon crucible brought about a lowering of the pressure during deposition since the outgassing of the graphite crucible was difficult to eliminate. Substrate temperatures between 100°C and 300°C represented the maximum temperature recorded by a thermocouple in contact with the back of a substrate during the deposition. Except when noted, the heating of the substrate was due to radiation from the crucible. In Samples 62 and 68, effort was made to deposit at high rates in order to limit the occlusion of residual gases. The residual atmosphere in the vacuum chamber was monitored with a mass analyzer. Typical partial pressures of major gases are shown in Table II.

Bulk boron was obtained from United States Mineral Company with the quoted purity of 99.99995. Attempts to crystallize the boron films by heating the samples in argon following the deposition have been unsuccessful. The films tend to crack and flake

off their substrate as they are crystallizing. Films deposited on substrates maintained at 900°C remain, however, continuous and smooth. The X-ray diffraction pattern of these films still shows diffuse rings.

III. Sputter-ion Source Mass Analysis

The films were analyzed by means of a sputter-ion source mass spectrometer*. This spectrometer employs a 10 kev argon ion beam which bombards the boron film, ejecting boron ions, boron ion clusters, ion complexes, and impurity ions from the film. The ejected ions are analyzed in a mass spectrometer. A typical mass spectrometer trace is shown in Fig. 2. The analysis of boron samples is very similar to that recently reported for silicon films [2]. Impurity analysis was carried out using an energy window of 100 eV and 250 eV. This allowed determination of atomic impurities without interference from clusters and complexes.

The impurity analysis of the films is obtained from the mass spectra by means of the following approximate equation:

$$f_{X^+} = \frac{I_{X^+} / Y_{X^+}}{I_{B^+} / Y_{B^+}}$$

where the I's represent ion contents, and Y's the relative ion yield. A knowledge of sputtering yields is thus essential for the determination of impurity content. Yields based on elements in elemental form are given in Table III, along with impurity analysis of the samples listed in Table I. If the impurities are assumed

* GCA Ion Microphobe Analytical Mass Spectrometer (IMS 101B), GCA Corp., Bedford, Mass.

to be in the oxidized state, the impurity content would be 10 - 15 times less.

The high content of carbon in Sample B-44 is clearly due to the graphite crucible. This is in contrast to statements found in the literature that the vapor pressure of carbon is much lower than that of boron at the melting point and consequently one does not expect many carbon impurities in the boron film [3]. The 8% carbon impurity in Sample 44 is considerably greater than the 0.2% equilibrium solubility of carbon in bulk boron. If the sample were crystallized, the carbon would probably reside on the grain boundaries as a separate C or B_4C phase [4]. Major impurities in the films (see B-68) tend to be silicon and iron. As can be seen from the tables, silicon may arrive from the source itself. The source of iron is more difficult to determine. Analysis of a different piece of bulk boron showed an iron contamination in small areas on the surface. The high silicon, oxygen, carbon and iron content of B-62A probably represents the SiO_2 showing through in pinholes as these impurities do not appear to the same extent in samples deposited on tantalum substrates. A direct comparison between series B-68 deposited on SiO_2 (not shown here) and on tantalum bears this out. Sample B-71 was deposited on a substrate held at 900° C. In this sample the silicon and iron as well as carbon and aluminum probably comes from diffusion from the substrate into the film. The fused silica substrate contains carbon and iron impurities as determined by the same mass analysis techniques. Care was taken during this high temperature run to

avoid heating any stainless steel since it had been shown that iron and chromium vapor could contaminate a sample at 900°C [2]. The samples do not appear to be contaminated with molybdenum or silver from the deposition crucible.

The carbon and oxygen impurities in all samples are difficult to analyze since there appears to be a surface reaction with the sample during sputtering in the mass analysis procedure. The carbon and oxygen impurity content in silicon films deposited by the same technique and at somewhat higher pressures are considerably less. McElligott and Roberts have demonstrated that O_2 and CO are chemisorbed strongly on a deposited boron film and this chemisorption appears to be greater than on silicon surfaces [5]. The amount of oxygen and carbon occluded in the films during deposition can not account for the large quantity of C and O observed. Table II shows the calculated values of the ratio of gas molecules striking the substrate/cm^2/sec, (ν_{gas}), to the boron atoms striking the surface/cm^2/sec, (ν_B). If all these gas molecules stick, which is unlikely, the sum of the oxygen-bearing species, assuming CO_2 and O_2 do not decompose, would give 434 ppm oxygen impurity in Sample B-68, while the mass analysis shows a 6000 ppm in Table III. The figures for O, C and perhaps N are thus too high.

IV. Boron Ion Cluster Analysis

The mass spectra shown in Fig. 2 show peaks corresponding to B_2^+ ... B_8^+. The peaks B_3 to B_8 have not been observed in the mass

spectra when a thermal source rather than sputter source is used [6]. The cluster peaks are complicated by the existence of two isotopes of almost equal intensity. A cluster of three boron atoms, for example, shows mass peaks at 30, 31, 32 and 33. The analysis of the clusters was accomplished by converting all peaks to an average main cluster $11_{B_n^+}$ peak through the prediction of relative intensities. The results are shown in Fig. 3, which shows the relative distribution of ion clusters ejected from the boron target. Note the deviations in the films from the relatively smooth distribution at B_5^+, which represents a cluster of 5 boron atoms. In the case of previously studied silicon films, the Si_4^+ ion deviated from the smooth distribution [2]. Using arguments discussed previously for silicon, and assuming that the distribution is related to short range order, one would draw the conclusion from these curves that the films contain a large fraction of boron with five nearest neighbors. The short range order in the amorphous films may thus be related to the α-rhombohedral phase as described by Badzian [7]. The cluster distribution in the films appears to differ from that of the bulk crystalline phase, however the analysis of crystallized film samples must be completed before more definite conclusions can be drawn.

V. Electrical Measurements

Electrical measurements were carried out on the samples described here in an effort to distinguish differences between

these pure samples and the ones described previously [8]. Resistance versus 1/T measurements were made in a pure argon atmosphere in a tube furnace with gravity contacts onto titanium deposited electrodes. The results are given in Fig. 4 for samples containing carbon, samples from a molybdenum crucible, and a sample deposited on a hot substrate. In each case, the curves could be broken into three straight lines representing three activation energies. Above 700°K, all of the samples appear to show an intrinsic slope of .65 eV. This would lead to a band gap of 1.3 eV, which is exactly that reported previously [8]. The activation energy at around 0.3 eV and 0.15 eV was also similar to those reported previously. There is thus little difference between the values of activation energies of more pure films and the films described earlier. These values are also similar to those found by various authors in crystalline boron [9]. The source of the activation energies is unknown, however it should be noted that the films may still contain a carbon impurity which could account for at least one of the energy levels [4].

All of the samples exhibit p-type conductivity and have a resistivity of 10^3 - 10^4 ohm-cm, measured by both a 2-contact and a 4-contact technique. The value is considerably lower than 10^{12} ohm-cm reported previously by us [8], and even lower than that reported for crystalline boron [10]. However, this low value of resistivity is the same as that found in carefully prepared films by "intrinsic thermometer method" [11]. The present films were deposited at 1000Å/min at less than 10^{-7} torr in contrast to the previous films deposited at 200Å/min at 2 x 10^{-5} torr. Also, as

discussed in Section III, these improved conditions have led to more pure films. The enormous decrease in resistivity with increased purity could then only be accounted for by the presence of large amounts of compensating impurities in the previous films and perhaps even in crystalline boron.

The previous samples deposited at 10^{-5} torr would readily switch from a low to a high conduction state in the manner previously described [12]. The low resitivity of the present samples makes switching difficult since it is hard to impose a high field. At liquid notrogen temperature, however, some switching does occur. The effects of joule heating and the analysis of pre-switching non-linear currents has been described elsewhere [13].

VI. Optical Measurements

The spectrophotometer used to measure transmission coefficient T is a double beam instrument in which the monochromatic beam from a SPEX Model 1400 double grating monochromator is divided by a beam splitter and allowed to pass through identical optical elements before being recombined and focused onto the detector. One leg of the beam is passed through the sample and the other through a reference absorber (usually air) before the beams are recombined. The sample and reference beams are chopped at two different frequencies (175 Hz and 200 hz) by tuning fork light choppers. The two frequency components of the detector signal are separated by two lock-in amplifiers in a manner such that a voltage proportional to the ratio of the sample signal intensity to the reference signal intensity is available for display on a strip chart recorder. The wavelength resolution of the instrument is a

function of wavelength and slitwidth. In all cases it is less than $5 \times 10^{-3}\mu m$ and is usually about $10^{-3}\mu m$. The photometric precision is T±0.005 over most of the range of the instrument. The photometric accuracy in the visible region, for which calibrated standards are available, is also T±0.005.

The optical constants were determined by measuring the transmission through two samples, deposited at the same time, which were identical except for thickness. The procedure for obtaining the optical constants from the transmission data has already been described elsewhere [1]. The value of the refractive index n at $\lambda = 2.5\ \mu m$ was found to be 3.45, which is to be compared with the value 3.1 for crystalline boron. This increase of approximately 10% is similar to the ones reported for amorphous forms of silicon [14,15], germanium[16] and many other covalently bonded semiconductors which have the same short range order in their crystalline and amorphous states.

The absorption coefficient α as a function of energy in the range of 0.6-1.7 eV is shown in Fig. 5 and compared with earlier results on amorphous boron [1]. For completeness, the data on single crystals of B-rhombohedral boron [17,18] is also included. The two sets of samples used in the present work were from 0.13 to 0.43 μm thick, allowing accurate measurements of transmission up to 1.7 eV. The absorption values in amorphous boron (Fig. 5) are higher than in the crystalline boron and the absorption edge is considerably broadened and shifted towards lower energies. The

situation is again similar to that in amorphous silicon [14,15,19] and germanium [16,20].

Compared to our previous data, the absorption coefficient is somewhat higher in the entire energy region; moreover, the sharper rise in absorption starting at 1.3 eV (see Fig. 5) is not discernible in the present data. The analysis of the data shows that the values of $\alpha \geq 10^4 cm^{-1}$, in the energy range 0.9 eV —1.65 eV, can be fitted very well to the expression

$$\alpha \propto \frac{(h\nu - E_g)^2}{h\nu}$$

with the "band gap" E_g = 0.62 eV. For lower values of α, the data can be fitted to an exponential $e^{h\nu/E_a}$ with the characteristic energy E_a = 0.12 eV. In terms of the recent models introduced to discuss the density of electronic states in disordered semiconductors, E_g corresponds to allowed optical transitions between band-like states, while E_a is an activation energy between states in the exponentially decaying tails of the density of states, induced by disorder. Though such models have been successfully applied to explain optical absorption in disordered semiconductor alloys and even in amorphous germanium and silicon, with admittedly less success, their usefulness is still a subject of lively controversy.

Conclusions

In the present paper, techniques for the production of relatively pure films of amorphous boron have been described. A quantitative method for determining impurity content and ion-

clustering effects in the films has been discussed. Elimination of the graphite crucible and the combination of lower deposition pressures and higher deposition rates has drastically reduced the carbon content of the films. The reduction in impurity content has, however, led to an enormous drop in the value of resistivity (by a factor of 10^8) as compared to the earlier films, and the values are even lower (by a factor of 10^2) than those reported for crystalline boron. It is therefore postulated that previous samples and perhaps crystalline boron contain a large amount of compensating impurities. This point needs further confirmation by deliberate doping of pure films with compensating impurities and checking the purity of crystalline boron. Such an analysis would also throw light on the effect of compensating impurities in the switching effect.

It should be noted that the reduced impurity content has not led to any significant changes in the thermal activation energies. The values of the activation energies, 0.15 eV, 0.35 eV and 0.65 eV are almost identical to those reported previously. This would indicate that the present films still contain the impurities responsible for the levels associated with these activation energies but the densities of these levels have been reduced. The highest activation energy for conduction (0.65 eV) found at temperatures exceeding 700°K would lead to a thermal gap of 1.3 eV. However, some caution should be exercised in the interpretation of this value or the smaller one obtained from optical measurements (0.62 eV) as a "band gap". The relationship

of these values to the concepts borrowed from band theory of crystalline solids is not entirely clear. Such large differences between the values of electrical and optical "band gap" are common when dealing with amorphous semiconductors and further work, particularly on the annealing of the samples, is planned to resolve them.

Acknowledgments

The authors are happy to acknowledge the work of Kenneth Hoggarth in depositing boron films, and of Frank Satkiewicz of GCA for carrying out the sputter-ion source mass spectra analysis.

REFERENCES

(1) K. Moorjani, C. Feldman,, Proc. of International Symposium on Boron, Warsaw, 1968, Electron Technology (Warsaw) 3, 265 (1970).

(2) C. Feldman, F. Satkiewicz, Thin Solid Films, 12, 217 (1972).

(3) K. Katada, Japanese J. App. Phys., 5, 582 (1966).

(4) O. A . Golikova, E. N. Nikitin, F. N. Tkalenko, Soviet Physics - Semiconductors, 4, 1193 (1971).

(5) P. E. McElligott, R. W. Roberts, J. Chem. Phys. 46, 273 (1967).

(6) M. G . Ingram, R. C. Porter, W. A. Chupha, J. Chem. Phys., 25, 498 (1956).

R. P. Burns, A. J. Jason, M. G. Ingram, J. Chem. Phys., 46, 394 (1967).

(7) A. R. Badzian, Refr. 1, page 143.

(8) C. Feldman, F. Ordway, W. Zimmerman III, K. Moorjani. Boron 2, Ed. Gaulé, Plenum Press, New York (1967).

(9) M. Prudenziati, G. Majini, A. A. Quaianta, J. Phys. Chem. Solids, 33, 245 (1972).

Sh. Z. Dzhamagidze, Yu. A. Mal'tsev, Soviet Physics - Semiconductors, 3, 80 (1969).

(10) D. Geist, J. Meyer and H. Peussner, Refr. 1, page 207.

G. V. Tsagareishvili, F. N. Tavadze, G. Sh. Darsavelidze and V. Sh. Metreveli, Refr. 1, p. 281.

E. I. Adirovich and L. M. Gol'dshtein, Soviet Phys. - Solid State 8, 1968 (1967).

(11) E. I. Adirovich and L. M. Gol'dshtein, Soviet Physics - Semiconductors, 3, 196 (1969).

(12) C. Feldman, W. A. Gutierrez, J. Appl. Phys., 39, 2747 (1968).

C. Feldman, K. Moorjani, J. Non-Crystalline Solids, 2, 82 (1970).

(13) K. Moorjani, C. Feldman, J. Non-Crystalline Solids, 4, 248 (1970).

(14) N. A. Blum, C. Feldman, K. Moorjani, Bull. Am. Phys. Soc., 17, 114 (1972)

(15) M. H. Brodsky, R. S. Title, K. Weiser, and G. D. Petit, Phys. Rev., B1, 2632 (1970).

(16) M. L. Theye, Optics Comm. 2, 329 (1970).

(17) E. Kierzek-Pecold, J. Kolodziejczak and I. Pracka, Phys. Stat. Sol. 22, K147 (1967).

(18) H. Werheit, A . Hausen and H. Binnenbruck, Phys. Stat. Sol. 42, 733 (1970).

(19) R. Grigorovici and A. Vancu, Thin Solid Films 2, 105 (1968).

(20) K. L. Chopra and S. K. Bahl, Phys. Rev. B1, 2545 (1970).

TABLE I

BORON DEPOSITION CONDITIONS

SAMPLE NO.	CRUCIBLE	VACUUM DURING DEPOSITION	DEPOSIT TIME (MIN)	t mμ	SUB TEMP °C	BEAM POWER kV	RATE Å/MIN	JAR	SUBSTRATES
B–44	C	2×10^{-6}	20	1.2	290	1.8	600	PYREX	Ta
B–60	Cu/Ag	8.5×10^{-8}	12.5	0.5	240	1.0	400	SS	Ta
B–62A	Mo	7.2×10^{-8}	3	0.36	200	2.0	1200	SS	SiO_2
B–68C	Mo	1.1×10^{-7}	4.5	0.59	300	1.2	1300	SS	Ta
B–71B	Mo	3×10^{-7}	6	0.29	900	1.1	485	SS	SiO_2

TABLE II

RESIDUAL ATMOSPHERE DURING BORON DEPOSITION
SAMPLE B–68

GAS	MASS	APPROXIMATE PARTIAL PRESSURE (torr)	ν_{gas}/ν_B (ppm)
CH_4	16	9×10^{-8}	1600
H_2O	18	4×10^{-9}	70
$CO + N_2$	28	1×10^{-8}	140
O_2	32	3×10^{-10}	4
C_nH_m	43	3×10^{-10}	3
CO_2	44	2×10^{-8}	220

TABLE III

APPROXIMATE MAJOR IMPURITY CONTENT IN BORON FILMS

SPECIES	YIELD (Y) 250 eV	YIELD (Y) 100 eV	BULK (100 eV)	B-44 (on Ta) (250 eV)	B-60 (on Ta) (250 eV)	B-62 (on SiO_2) (250 eV)	B-68 (on Ta) (100 eV)	B-71 (on SiO_2) (100 eV)
C(BH)*	2	2	B(?)	88,000	2,600	2,900	~300	~5,000
N*	7	5.9	B(?)	90	130	90	~100	~300
O*	~.3	1.9	B(?)	9,000	9,000	>10,000	6,000	~35,000
Na	200	115	ND	10	23	3	12	12
Mg	20	6	ND	ND	15	ND	20	80
Al(BO)	22	22	30	18	30	40	40	800
Si	3.3	3.3	100	<100	95	1,200	160	1,400
K	1,200	6.9	0.4	0.5	0.5	0.6	0.7	1
Ca	25	100	7	32(I Ar)	ND(I)	ND(I)	24	16
Ti	37	37	ND	21	4	ND	ND	ND
V	3.7	3.7	ND	~15	80	ND	50	ND
Cr	10	10	ND	ND	< 5	80	20	80
Fe	1.9	1.9	ND	<180	80	440	140	800
B	10	10						

ND = Not Detected

I = Interference

* = Background (B) subtracted

Figure Captions

Fig. 1 Arrangement in bell jar showing source crucible with molybdenum liner and electron gun.

Fig. 2 Polyatomic mass spectrum of a boron film (Sample 68-C).

Fig. 3 Relative distribution of B_n^+ ion clusters from bulk and three different films of boron.

Fig. 4 Resistance as a function of reciprocal temperature for three different films of boron.

Fig. 5 Optical absorption coefficient as a function of energy.

——— present data on amorphous boron

— — — previous data on amorphous boron (Refr. 1)

— - — data on crystalline boron (Refr. 17)

— -- — data on crystalline boron (Refr. 18)

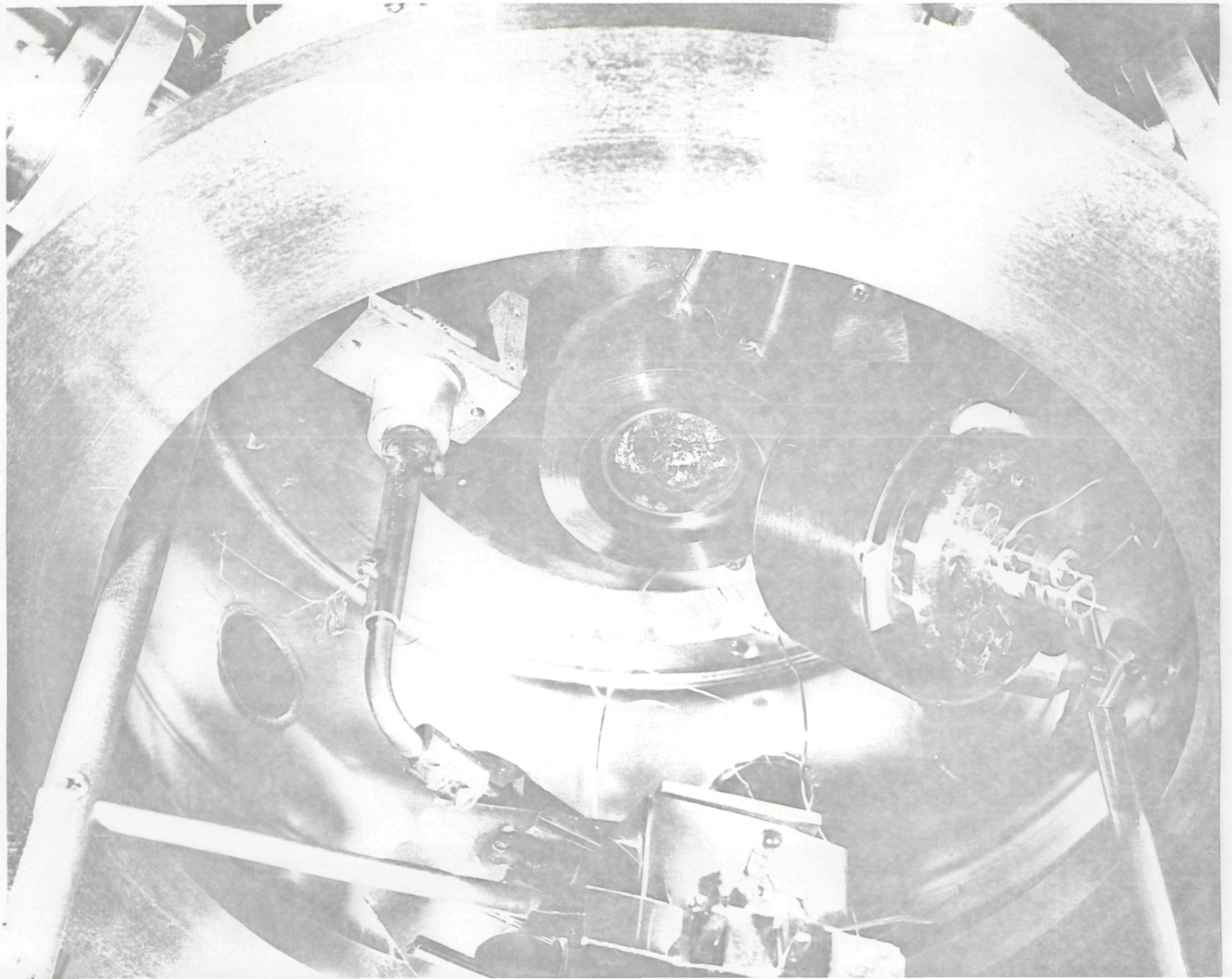

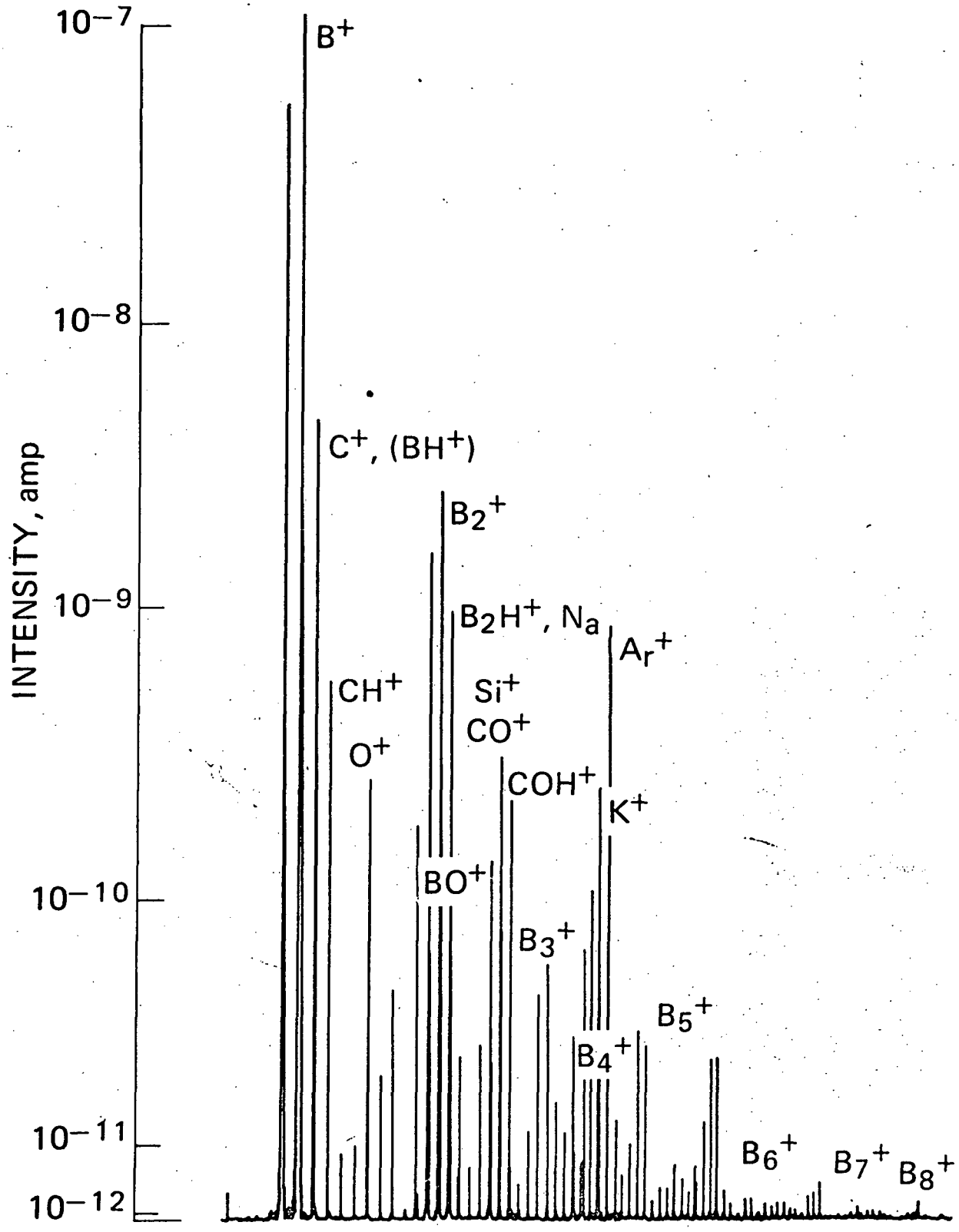
INTENSITY, amp
10−7
10−8
10−9
10−10
10−11
10−12
B+
C+, (BH+)
B2+
B2H+, Na
Ar+
CH+
Si+
O+
CO+
COH+
K+
BO+
B3+
B5+
B4+
B6+
B7+
B8+

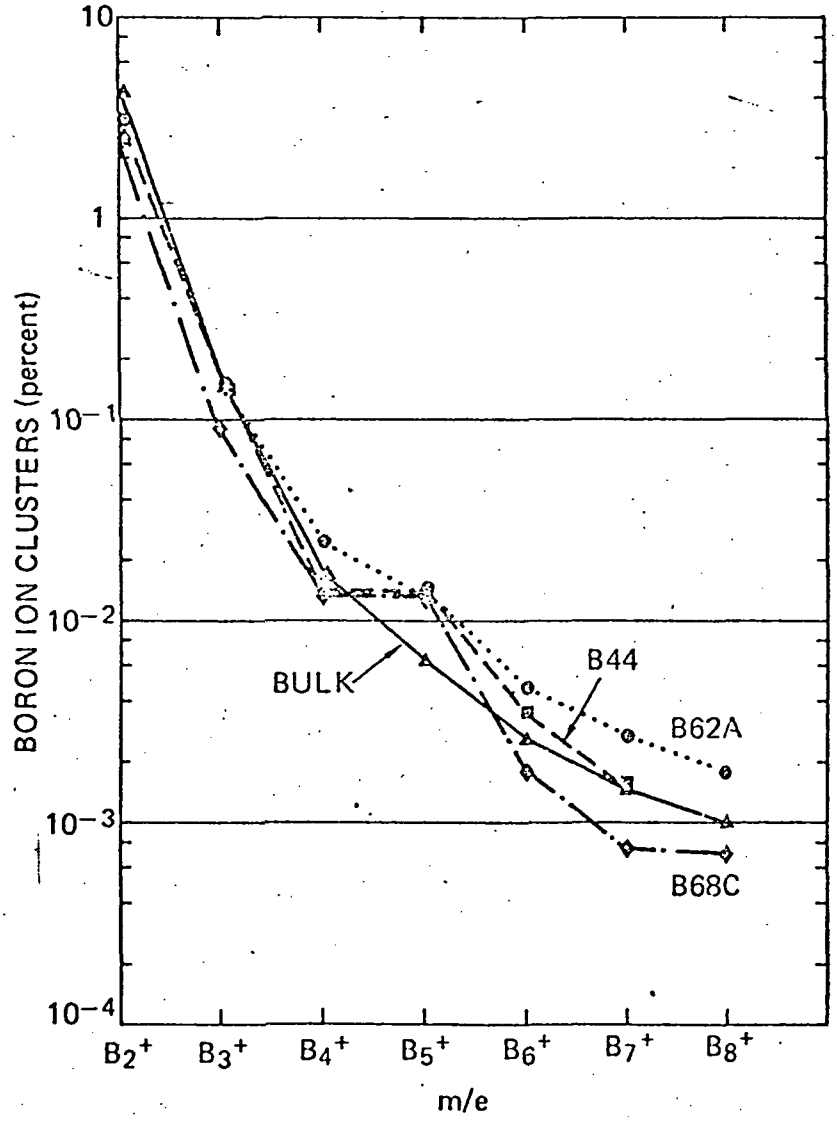
10
1
10^{-1}
10^{-2}
10^{-3}
10^{-4}
BORON ION CLUSTERS (percent)
BULK
B44
B62A
B68C
B_2^+
B_3^+
B_4^+
B_5^+
B_6^+
B_7^+
B_8^+
m/e

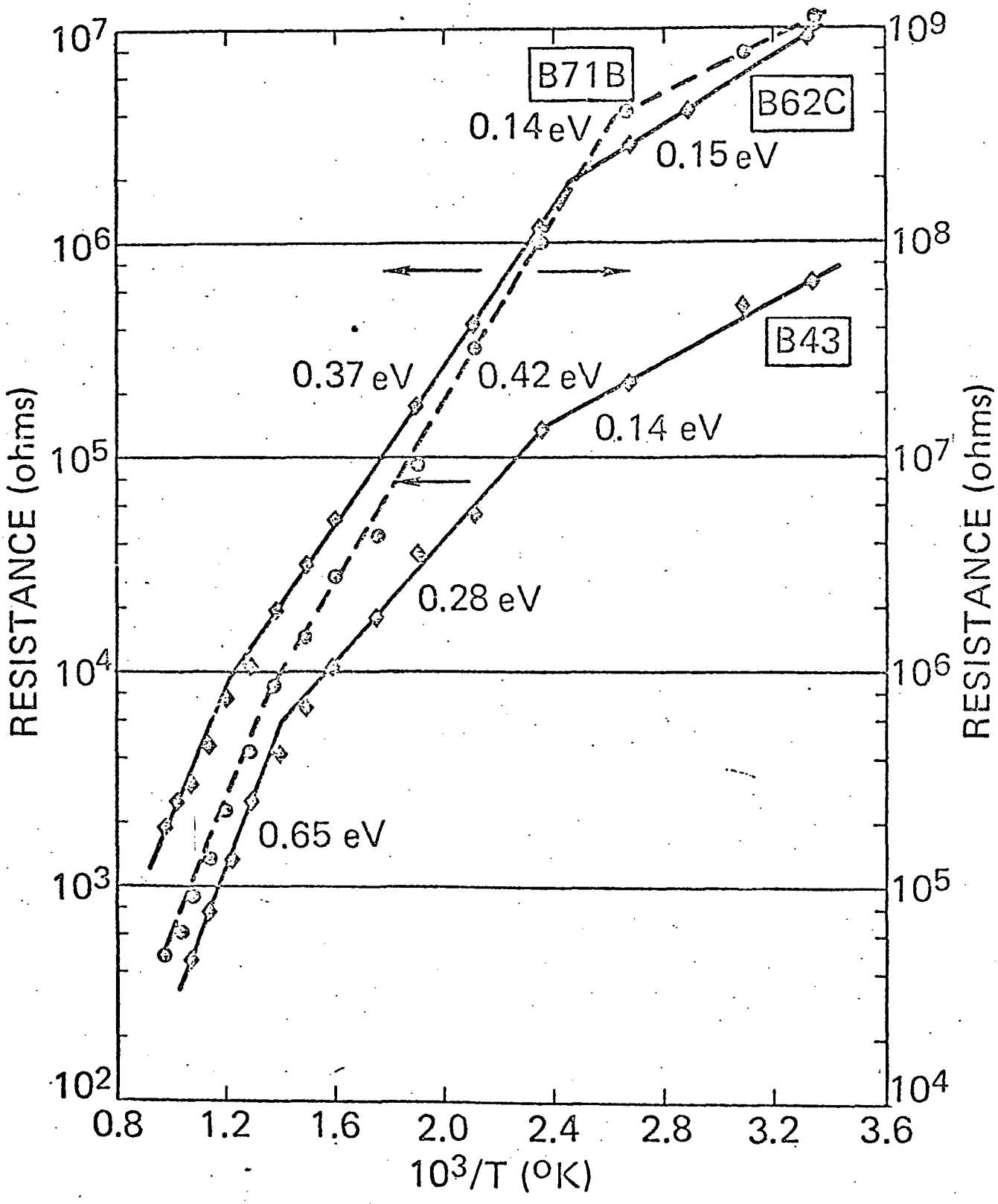
B71B
B62C
B43
0.14 eV
0.15 eV
0.37 eV
0.42 eV
0.14 eV
0.28 eV
0.65 eV
RESISTANCE (ohms)
RESISTANCE (ohms)
10^7
10^6
10^5
10^4
10^3
10^2
10^9
10^8
10^7
10^6
10^5
10^4
0.8
1.2
1.6
2.0
2.4
2.8
3.2
3.6
$10^3/T$ (°K)

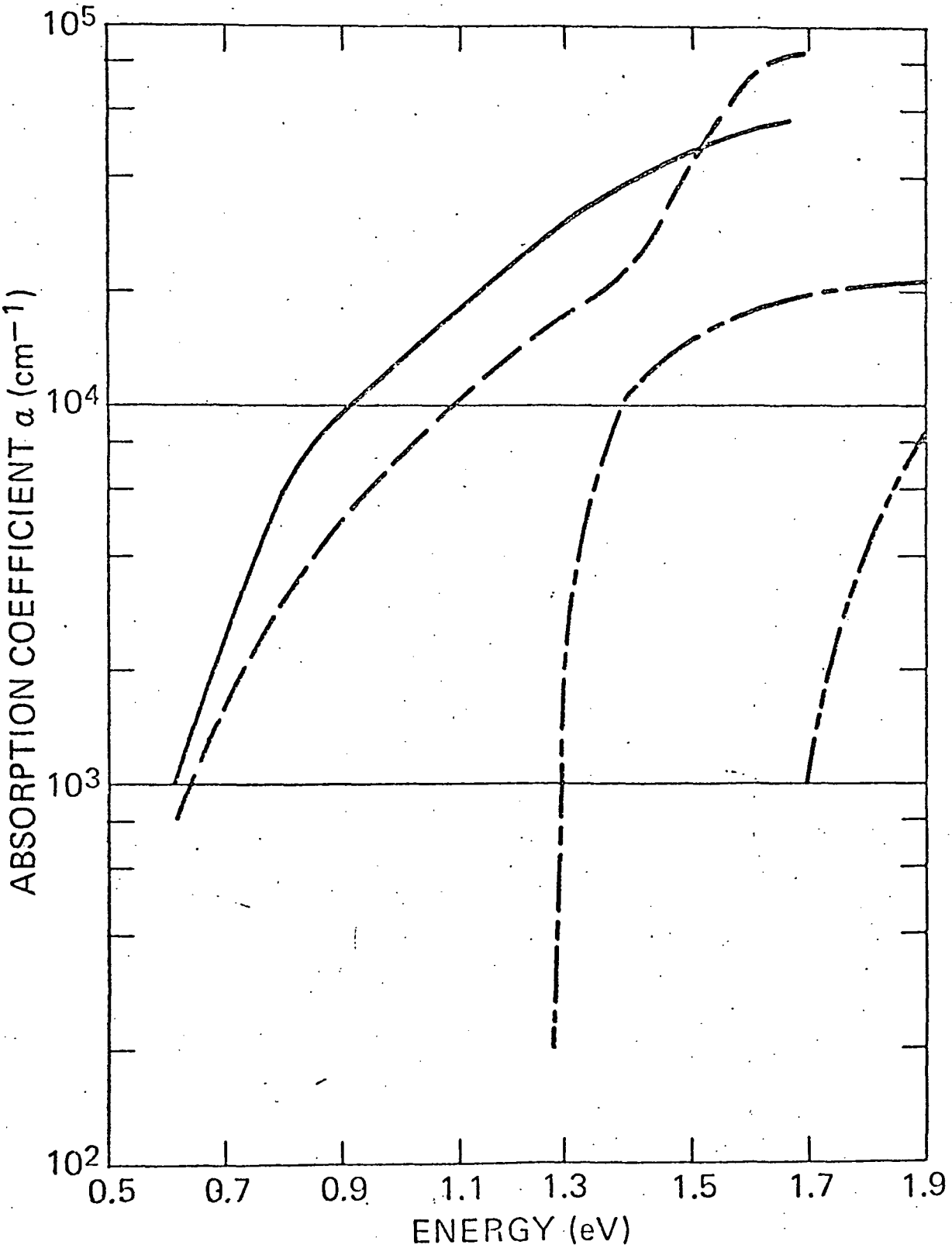
10^5
10^4
10^3
10^2
ABSORPTION COEFFICIENT α (cm^{-1})
0.5
0.7
0.9
1.1
1.3
1.5
1.7
1.9
ENERGY (eV)

APPENDIX III

JOURNAL OF NON-CRYSTALLINE SOLIDS 11 (1972) 242–246 © North-Holland Publishing Co.

LETTERS TO THE EDITOR

THE CRYSTALLIZATION OF AMORPHOUS SILICON FILMS*

NORMAN A. BLUM and CHARLES FELDMAN

Applied Physics Laboratory, The Johns Hopkins University, 8621 Georgia Avenue, Silver Spring, Maryland 20910, U.S.A.

Received 31 May 1972

It is well known that the heating of vacuum deposited amorphous silicon films above about 700°C produces an irreversible transformation to the crystalline state[1,2]). Films deposited on substrates near or below room temperature may, furthermore, tend to contain voids[3]). At higher substrate temperatures the relative volume of voids diminishes, but the films may begin to crystallize. The lowest practical crystallization temperatures and times should be used to avoid introduction of impurities. It is therefore important to know in some detail how deposition temperature and subsequent annealing influence the approach to crystallinity in amorphous silicon films. The crystallization process has been followed by observing optical transmission changes in the films as they are heated at various temperatures. It will be shown that the crystallization process is a gradual one which takes place at any finite temperature. Heat treatment which is likely to anneal away the voids is also likely to make the sample tend toward crystallinity.

The samples were prepared by electron beam vacuum deposition onto pure fused silica substrates at about 2×10^{-7} torr at rates from 200 to 300 Å/ /min with the substrate temperature rising from 200°C to 300°C during the deposition. Pre-deposition pressure was about 5×10^{-9} torr. The source to substrate distance was about 15 cm. For the experiments described here, the film thicknesses were approximately 5000 Å. Film thicknesses were measured by a multiple beam interference technique and revealed a decrease in thickness, and thus also in the volume, in going from amorphous to crystallized samples, of about 8.2%. Samples were heated in a tube furnace flowing with pure argon for a fixed time and temperature and then removed from the furnace and examined optically.

* Work supported by NASA under Grant No. NGR 21-009-033 and by Naval Ordnance Systems Command, Contract N00017-72-C-4401, Task A13B.

For incident photon energies above about 2.0 eV both amorphous and crystallized Si films are heavily absorbing. At 2.6 eV, for example, crystalline films exhibit an absorption coefficient α of about 2×10^4 cm^{-1}, while "as deposited" (amorphous) films show an α at least three orders of magnitude greater. Thus, the transmission of the films at 2.6 eV (4800 Å) is a sensitive indication of the degree of crystallinity or amorphicity. An arbitraty criterion for "onset of crystallinity" used here is that 5000 Å thick samples have a total external transmittance of 5% (corresponds approximately to $\alpha=6\times10^4$) at a wavelength of 4800 Å. Samples meeting this criterion are nearly crystallized; further heating results in only a slight increase in transmission. The results are independent of the exact details of the criterion as long as it gives an indication of a phase state somewhere between the two extremes; a criterion based upon maximum rate of change of the observed parameter with annealing is clearly most useful. In practice, since the sample transmission was not monitored during the annealing process, the times are approximate. The operational procedure was to estimate the time to reach the criterion and anneal for that length of time at constant temperature. If the criterion was not met (i.e., the transmission at 4800 Å was appreciably different from 5% at 4800 Å), then the anneal was repeated with another sample at the same temperature for a shorter or longer time depending on whether the sample was on the amorphous or crystalline side of meeting the criterion. The procedure was repeated until a satisfactory result was obtained.

Using the above criterion, the time to reach "onset of crystallinity" t_c was determined as a function of annealing temperature T for a sample which was divided into pieces, each annealed and analyzed separately. This assured that all samples started out identical to one another. The plot of log t_c versus T^{-1}, shown in fig. 1, gives a straight line, indicating that the simple rate expression

$$t_c = \tau \exp(E_0/kT) \tag{1}$$

is a reasonable approximation relating t_c and T. Above and to the left of the line is the area of certain crystallinity, below and to the right lies the area of amorphicity. Close to the line is the intermediate region where the sample is in transition between the two states.

In eq. (1), τ is associated with the characteristic time of a microscopic interaction between neighboring atoms, while E_0 is identified with the activation energy between the metastable amorphous state and the stable crystalline state. From fig. 1, $\tau\simeq5\times10^{-14}$ sec and $E_0\simeq3.1$ eV, both figures are reasonably consistent with the identification of τ as an interaction time between atomic neighbors and E_0 as an activation energy for self diffusion in Si [4]).

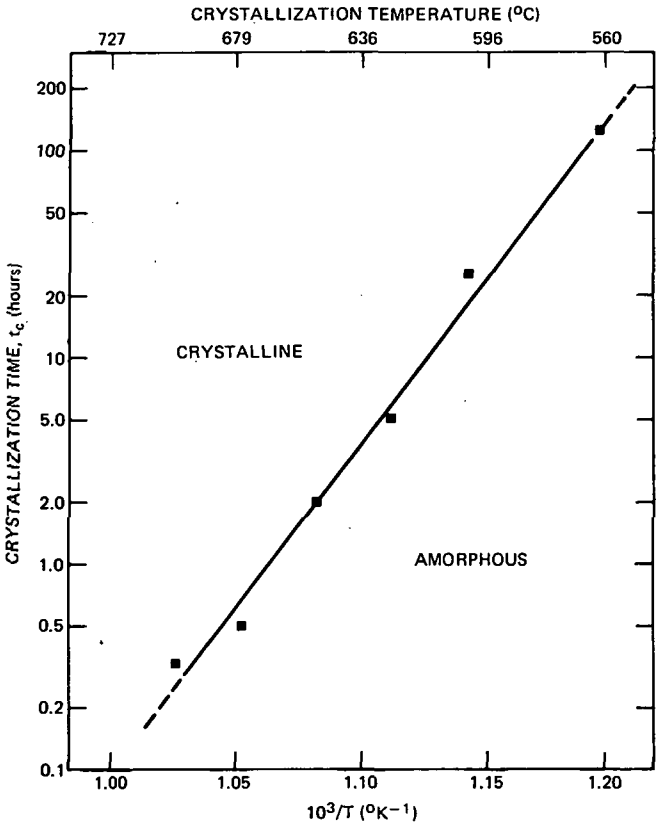

Fig. 1. Plot of crystallization time versus the reciprocal annealing temperature, showing regions where sample remains mostly amorphous and where it is crystallized.

The plot in fig. 1 applies only to films prepared between 200 °C and 300 °C. The detailed behavior probably also depends on the nature of the substrate and other preparation parameters. Films deposited on higher temperature substrates show evidence of being already partially crystallized. For a film deposited at 500 °C we observed points below those shown in fig. 1, indicating that preannealing had taken place.

Eq. (1) has a form common to many polymorphic transformations which do not include nucleation[5]). The same short range order prevails in both amorphous and crystalline form – both structures contain silicon tetrahedra. The transformation consists of a displacement of silicon atoms from metastable sites over a potential barrier E_0 to lower energy crystal sites. In the film, this produces a polycrystalline structure with small grain size.

If the volume of the film in the crystalline phase is V_c and the volume

transforming is proportional to the untransformed volume, then the rate of transformation is

$$\frac{dV_c}{dt} = k_0 (V - V_c);$$

so that

$$V_c = V[1 - \exp(-k_0 t)], \quad (2)$$

where V is the total volume; and k_0 is the rate constant,

$$k_0 = \nu \exp(-E_0/kT). \quad (3)$$

From (2), the fraction corresponding to the crystallinity condition which is untransformed at a time t_c is

$$g = \frac{V - V_c}{V} = \exp(-k_0 t_c). \quad (4)$$

The time t_c corresponds to the observed optical criterion for crystallinity at a temperature T, and thus determines some untransformed fraction g; this constant fraction may be combined with (3) and (4) to give

$$t_c = \tau \exp(E_0/kT), \quad (1)$$

where $\tau = \nu^{-1} |\log g|$ and has the interpretation mentioned previously.

A plot such as that shown in fig. 1 is very useful for experimenters wishing to anneal films while: (a) preserving most of the amorphous character; or (b) crystallizing the sample without unnecessarily risking contamination or physical damage by overtreatment. It should be emphasized that such a plot applies in detail only to samples prepared under a given set of conditions; for other preparation parameters the slope and intercept of the $\log t$ versus T^{-1} line would be different from that shown in fig. 1. The results show that the change from a-Si to c-Si is a gradual one which, to a first approximation, may be described by eq. (1). At room temperature the amorphous film is stable; using the experimentally derived constants, the time for crystallization of an amorphous film at 300 K is $\simeq 3 \times 10^{33}$ years!

The authors are pleased to acknowledge the capable technical assistance of Messrs. K. Hoggarth and E. Koldewey in carrying out the work reported here.

References

1) R. Grigorovici, Mater. Res. Bull. 3 (1968) 13.
2) M. H. Brodsky, R. S. Title, K. Weiser and G. D. Petit, Phys. Rev. B 1 (1970) 2632, and references therein. The gradual transition as revealed by the optical transmission from

a-Si to c-Si as a function of annealing temperature can be seen from fig. 4 of thi reference. For their preparation parameters and crystallization criteria, Brodsky et al report that the film crystallized during the 500°C annealing cycle.

3) T. M. Donovan and K. Heinemann, Phys. Rev. Letters **27** (1971) 1794; F. L. Galeener, Phys. Rev. Letters **27** (1971) 1716.
4) A. Seeger and M. L. Swanson, in: *Lattice Defects in Semiconductors*, Ed. R. R. Hasi guti (Univ. of Tokyo Press, 1968) p. 125.
5) J. W. Christian, *The Theory of Transformations in Metals and Alloys* (Pergamon Oxford, 1965) pp. 16–22.

APPENDIX IV

Reprinted from the Proceedings of the

Second International Conference on
CONDUCTION IN LOW-MOBILITY MATERIALS

EILAT, ISRAEL
5–8 April 1971

TAYLOR & FRANCIS LTD
International Scientific Publishers
10–14 Macklin Street, London WC2B 5NF

Pair Approximation in the Coherent Potential Theory of Disordered Solids

By K. MOORJANI†
Applied Physics Laboratory, The Johns Hopkins University, 8621 Georgia Avenue, Silver Spring, Maryland 20910
and T. TANAKA‡
Catholic University of America, Washington, D.C. 20017
and S. M. BOSE‡
Drexel University, Philadelphia, Pennsylvania, 19026§, and Catholic University of America, Washington, D.C. 200017

ABSTRACT

The paper develops a self-consistent method for studying disordered systems with diagonal as well as off-diagonal disorder. The method has general applicability to any disordered system and in the present analysis is applied to a monoatomic system where disorder arises due to a random distribution of vacancies.

§ 1. INTRODUCTION

THE equilibrium and the non-equilibrium aspects of disordered solids have attracted a great deal of attention recently, experimentally as well as theoretically. (See various papers in the proceedings edited by Mott 1970.) In particular, many different theoretical approaches are available for discussing the properties of disordered binary alloys. The principal among these is the recently introduced coherent-potential approximation (CPA) by Soven (1967).

The application of the CPA to a disordered binary alloy is based on replacing the atomic potential at each lattice site by an undetermined coherent potential. The multiple scattering effects from the actual potentials are described via a T-matrix, where the scattering potential is the difference between the actual potential and the coherent potential. In an exact formulation the coherent potential can be determined self-consistently from the condition that the configurational average of the T-matrix must vanish. In the CPA this condition is replaced by a weaker one requiring the configurational average of the atomic T-matrix to vanish.

† Partially supported by Naval Ordnance Systems Command, Contract No. NOw–62–0604–c, Task A13B, and NASA Grant No. NGR–21–009–033.
‡ Supported by National Aeronautics and Space Administration Research under Grant No. NASA NGR–09–005–072.
§ Present address.

The success of the CPA is evidenced by a number of recent papers which have used the CPA to discuss the static and the dynamic aspects of disordered alloys (Velický, Kirkpatrick and Ehrenreich 1968, Velický 1969, Velický and Levin 1970, Kirkpatrick, Velický and Ehrenreich 1970, Economou, Kirkpatrick, Cohen and Eggarter 1970, Stroud and Ehrenreich 1970, Soven 1970). The method, however, is applicable to alloys possessing diagonal disorder only, thus making it useful mainly for alloys composed of isoelectronic atoms. Recently, attempts have been made to include off-diagonal randomness in approximations similar to the CPA (Berk 1970, Foo, Amar and Ausloos 1970).

In the present analysis a more general self-consistent approach is developed which is capable of dealing with solids exhibiting diagonal as well as off-diagonal disorder. The general ideas followed are similar in nature to those in the CPA. The off-diagonal randomness arises due to the randomness in the hopping energy of an electron between nearest-neighbour atoms. This necessitates the introduction of a wave-vector dependent coherent potential in contrast to the wave-vector independent coherent potential of the single-site CPA.

The model and the formalism are described in the next section and the results are discussed in the last section.

§ 2. Formalism

The present formalism concerns itself with the effect of diagonal and off-diagonal disorder on the electronic density of states of a one-band system. The method has general applicability but we focus our attention on a monoatomic system. The disorder in such a one-component system can be simulated by removing a certain fraction of atoms at random, from an ordered lattice. The probability of occupation of a given lattice site is then given by $c(0<c<1)$, where $c=1$ represents the completely ordered lattice.

We write the total Hamiltonian for the above system as a sum of Hamiltonians describing the pairwise interaction of a given particle with its nearest neighbours.

$$\mathscr{H}=\sum_{\alpha}\mathscr{H}_{\alpha}, \quad . \quad . \quad . \quad . \quad . \quad . \quad . \quad . \quad . \quad (1)$$

where the summation is over all nearest-neighbour pairs α and

$$\mathscr{H}_{\alpha}=\mathscr{H}_{lm}=W_{ll}a_l^*a_l+W_{mm}a_m^*a_m+W_{lm}(a_l^*a_m+a_m^*a_l). \quad . \quad (2)$$

Here $W_{ll}=\frac{\epsilon}{z}\mu_l$ and $W_{lm}=W\mu_l\mu_m=W_{ml}$. The disorder is incorporated through the variable μ, which is unity for an occupied site and zero otherwise. In the above definitions, ϵ denotes the potential energy at each lattice site while W is the hopping energy between two nearest neighbours. Finally z is the number of nearest neighbours.

The equilibrium quantity of interesst is the electronic density of states $\rho(E)$, given by the well-known expression

$$\rho(E) = -\frac{1}{\pi} \text{ Im Trace } \bar{G}(E), \quad . \quad . \quad . \quad . \quad . \quad . \quad (3)$$

where the functional dependence of the Green's function on the complex energy E is given by

$$G(E) = \frac{1}{E - \mathscr{H}} \quad . \quad . \quad . \quad . \quad . \quad . \quad . \quad . \quad (4)$$

and the bar denotes the average over all possible configurations of the system.

To discuss the effects of multiple scattering of an electron from systems represented by the Hamiltonian (1), we introduce an effective medium described by the Hamiltonian,

$$\Sigma = \sum \Sigma_0(a_l^* a_l + a_m^* a_m) + \Sigma_1(a_l^* a_m + a_m^* a_l), \quad . \quad . \quad . \quad (5)$$

where $\Sigma_0 (= \Sigma_{ll})$ and $\Sigma_1 (= \Sigma_{lm})$ are respectively the diagonal and the off-diagonal coherent potentials, as yet undetermined. It is desirable that Σ_0 and Σ_1 be determined self-consistently.

The multiple-scattering effects are now easily described by the T-matrix,

$$T = (\mathscr{H} - \Sigma)[1 + \bar{G}T], \quad . \quad . \quad . \quad . \quad . \quad . \quad (6)$$

where the configurationally averaged Green's function is given by

$$\bar{G}(E) = \frac{1}{E - \Sigma}. \quad . \quad . \quad . \quad . \quad . \quad . \quad . \quad (7)$$

From the relationship

$$G = \bar{G} + \bar{G}T\bar{G}, \quad . \quad . \quad . \quad . \quad . \quad . \quad . \quad (8)$$

we note that the configurational average of the T-matrix must vanish. That is,

$$\bar{T} = 0. \quad . \quad . \quad . \quad . \quad . \quad . \quad . \quad (9)$$

The eqn. (9) represents the self-consistent condition which determines the coherent potentials Σ_0 and Σ_1; which in turn determine the density of states via eqns. (7) and (3).

In the above analysis the problem has been treated exactly, but to proceed any further some approximations are needed. In the CPA, the condition represented by eqn. (9) was replaced by a simpler one requiring the configurational average of the atomic T-matrix to vanish. Such a single-site approximation was adequate to determine the single, k-independent, coherent potential introduced there. Below we discuss the two-sites approximation appropriate to the system represented by the Hamiltonian (1).

The full T-matrix (eqn. (6)) can be written in terms of two-sites t-matrices by the conventional expression,

$$T=\sum_{\alpha} t_{\alpha}+\sum_{\alpha\neq\beta} t_{\alpha}\bar{G}t_{\beta}+\sum_{\alpha\neq\beta\neq\gamma} t_{\alpha}\bar{G}t_{\beta}\bar{G}t_{\gamma}+,\ldots \quad (10)$$

where the two-sites t-matrix is given by

$$t_{\alpha}=(\mathscr{H}_{\alpha}-\Sigma_{\alpha})[1+Gt_{\alpha}]. \quad (11)$$

In eqn. (10), the restricted summations imply that the successive pair indices cannot be equal; that is, in the third term $\alpha\neq\beta$ and $\beta\neq\gamma$ but $\alpha=\gamma$ is allowed.

The self-consistent condition (9) is now replaced by a weaker one,

$$\bar{t}_{\alpha}=0. \quad (12)$$

This matrix equation leads to two equations, one for the diagonal matrix elements ($\bar{t}_{mm}=0$) and the other for the off-diagonal matrix elements ($\bar{t}_{lm}=0$) and they determine the two unknowns Σ_0 and Σ_1.

In Wannier representation, the matrix elements of the t-matrix are written as

$$t_{lm}=(W_{lm}-\Sigma_1)+(W_{ll}-\Sigma_0)[g_0t_{lm}+g_1t_{mm}]+(W_{lm}-\Sigma_1)[g_1t_{lm}+g_0t_{mm}] \quad (13)$$

and

$$t_{mm}=(W_{mm}-\Sigma_0)+(W_{ml}-\Sigma_1)[g_0t_{lm}+g_1t_{mm}]+(W_{mm}-\Sigma_0)[g_1t_{lm}+g_0t_{mm}], \quad (14)$$

where l and m are nearest neighbours. The quantities $g_0(=\bar{G}_{mm})$ and $g_1(=\bar{G}_{lm})$ are obtained from the matrix elements of the Green's function,

$$\bar{G}_{lm}(E)=\frac{1}{N}\sum_{k}\frac{\exp\,[ik\,.\,(l-m)]}{E-z\Sigma_0-\gamma(k)\Sigma_1}. \quad (15)$$

In eqn. (15), the structure factor $\gamma(k)=\sum_{\Delta}\exp\,(ik\,.\,\Delta)$, where Δ is the nearest-neighbour vector.

Equations (13) and (14) can now be solved for t_{mm} and t_{lm} and the requirement that their configurational averages vanish, leads to the equations

$$0=\frac{c^2}{D_1}\left\{\left[(W-\Sigma_1)^2-\left(\frac{\epsilon}{z}-\Sigma_0\right)^2\right]g_0+\left(\frac{\epsilon}{z}-\Sigma_0\right)\right\}+\frac{2c(1-c)}{D_2}\left\{\left[\Sigma_1{}^2+\Sigma_0\left(\frac{\epsilon}{z}-\Sigma_0\right)g_0+\left(\frac{\epsilon}{2z}-\Sigma_0\right)\right]\right\}+\frac{(1-c)^2}{D_3}\{(\Sigma_1{}^2-\Sigma_0{}^2)g_0-\Sigma_0\} \quad (16)$$

and

$$0=\frac{c^2}{D_1}\left\{\left[(W-\Sigma_1)^2-\left(\frac{\epsilon}{z}-\Sigma_0\right)^2\right]g_1-(W-\Sigma_1)\right\}$$
$$+\frac{2c(1-c)}{D_2}\left\{\left[\Sigma_1{}^2+\Sigma_0\left(\frac{\epsilon}{z}-\Sigma_0\right)\right]g_1+\Sigma_1\right\}$$
$$+\frac{(1-c)^2}{D_3}\{[\Sigma_1{}^2-\Sigma_0{}^2]g_1+\Sigma_1\}, \quad (17)$$

where

$$D_1=(g_0{}^2-g_1{}^2)\left[(W-\Sigma_1)^2-\left(\frac{\epsilon}{z}-\Sigma_0\right)^2\right]$$
$$+2(W-\Sigma_1)g_1+2\left(\frac{\epsilon}{z}-\Sigma_0\right)g_0-1, \quad (18\,a)$$

$$D_2=(g_0{}^2-g_1{}^2)\left[\Sigma_1{}^2+\Sigma_0\left(\frac{\epsilon}{z}-\Sigma_0\right)\right]-2\Sigma_1 g_1+\left(\frac{\epsilon}{z}-2\Sigma_0\right)g_0-1 \quad (18\,b)$$

and

$$D_3=(g_0{}^2-g_1{}^2)[\Sigma_1{}^2-\Sigma_0{}^2]-2\Sigma_1 g_1-2\Sigma_0 g_0-1. \quad (18\,c)$$

The formulation is now complete since eqns. (16) and (17) can, in principle, be solved for the two unknowns Σ_0 and Σ_1 in terms of ϵ, W and the energy E. The density of states in terms of Σ_0 and Σ_1 is easily obtained by rewriting eqn. (3) as

$$\rho(E)=-\frac{N}{\pi}\,\mathrm{Im}\,\bar{G}_{mm}(E)=-\frac{N}{\pi}\,\mathrm{Im}\,g_0, \quad (19)$$

or

$$\rho_{\mathrm{at.}}(E)=-\frac{1}{\pi}\,\mathrm{Im}\,g_0, \quad (20)$$

where $\rho_{\mathrm{at.}}(E)$ is the density of states/atom and g_0 is obtained from eqn. (15).

The numerical solution of eqns. (16) and (17) for a three-dimensional solid is not entirely simple. The corresponding calculations are now underway and will be reported in the near future. However, the simpler problem of one-dimensional disorder chain lends itself to an exact analytic solution in the present formulation and is discussed in the next section.

§ 3. Results

For the case of one-dimensional chain, eqns. (16) and (17) can be decoupled to obtain a quartic equation for $p=(2Wg_0)^{-1}$, written below in the form of a dispersion equation,

$$\frac{1}{p}-\left[\frac{c^2}{p+x-1}+\frac{c^2}{p+x+1}+\frac{2c(1-c)}{p+x}+\frac{2(1-c)}{p+x+\delta}\right]=0, \quad (21)$$

where $x=E-\epsilon/2W$ and $\delta=\epsilon/2W$. In these units, the band for an

ordered chain ($c=1$) is centred at the origin with the half-bandwidth equal to unity.

The numerical values of the density of states/atom (actually $\rho_{at.}' = \pi 2W\rho_{at.}$) obtained from the solution of eqn. (21) are plotted in the figure. For ordered lattice ($c=1$), $\rho(x)$ has the well-known symmetric shape with singularities at the band edges ($x=\pm 1$). As soon as c deviates from unity the singularities disappear, the main band narrows and a band associated with the vacancies appears below the main band. As expected (figure), the increasing value of δ leads to the shift of the centre of the ' vacancy ' band away from the lower edge of the main band and also causes its broadening. The broadening also results from increasing disorder represented by decreasing value of c.

Fig. 1

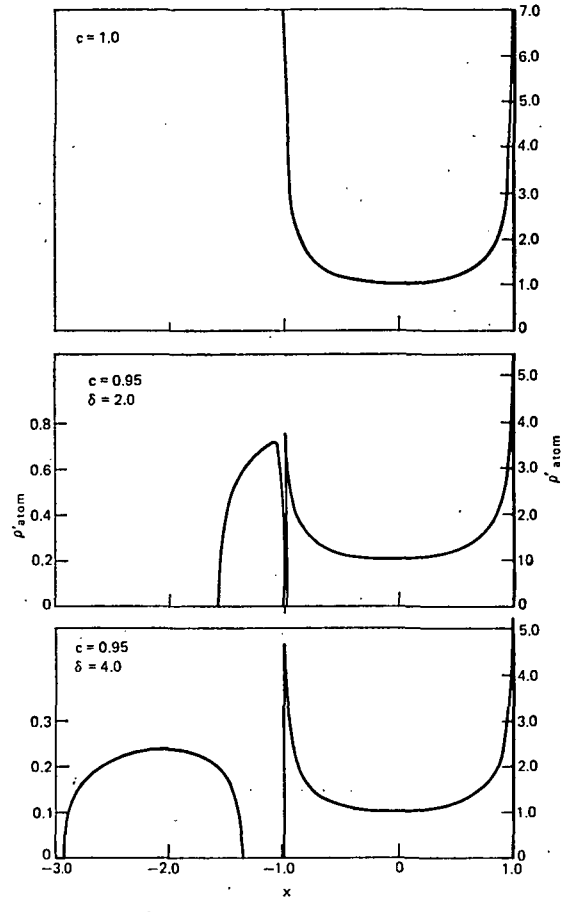

The density of states/atom (in units of $2\pi W$) versus normalized energy $x=E-\epsilon/2W$. The scale on the right refers to the main band and that on the left to the ' vacancy ' band.

The important question of whether these states, for a three-dimensional disordered solid, are localized in nature, can only be answered by calculating conductivity. Such a calculation, in the formulation presented here, is now under way.

ACKNOWLEDGMENTS

K. Moorjani would like to express his sincere thanks to S. Favin of the Applied Physics Laboratory for his help with the computer programming.

REFERENCES

BERK, N. F., 1970, *Phys. Rev.* B, **1,** 1336.
ECONOMOU, E. N., KIRKPATRICK, S., COHEN, M. H., and EGGARTER, T. P., 1970, *Phys. Rev. Lett.*, **25,** 520.
FOO, E-NI., AMAR, H., and AUSLOOS, M., 1970, *Bull. Am. phys. Soc.*, **15,** 774.
KIRKPATRICK, S., VELICKÝ, B., and EHRENREICH, H., 1970, *Phys. Rev.* B, **1,** 3250.
MOTT, N. F., 1970, *Proc. Int. Conf. on Amorphous and Liquid Semiconductors*, Cambridge, England.
SOVEN, P., 1967, *Phys. Rev.*, **156,** 809 ; 1970, *Ibid.*, B **2,** 4715.
STROUD, D., and EHRENREICH, H., 1970, *Phys. Rev.* B, **2,** 3197.
VELICKÝ, B., 1969, *Phys. Rev.*, **184,** 614.
VELICKÝ, B., KIRKPATRICK, S., and EHRENREICH, H., 1968, *Phys. Rev.*, **175,** 747.
VELICKÝ, B., and LEVIN, K., 1970, *Phys. Rev.* B, **2,** 938.

APPENDIX V

JOURNAL OF NON-CRYSTALLINE SOLIDS 8–10 (1972) 155–159 © North-Holland Publishing Co.

COHERENT POTENTIAL THEORY OF OFF-DIAGONAL RANDOMMESS: BINARY ALLOY

T. TANAKA and M. M. SOKOLOSKI*†
Department of Physics, The Catholic University of America, Washington, D.C. 20017, U.S.A.

K. MOORJANI**
Applied Physics Laboratory, The Johns Hopkins University, Silver Spring, Maryland 20910, U.S.A.

and

S. M. BOSE*
Department of Physics, Drexel University, Philadelphia, Pennsylvania 19026, U.S.A.

The single-site coherent potential approximation (SS-CPA) for a disordered binary alloy is extended in a self-consistent manner to the case of off-diagonal randomness. The density of states for a bcc lattice is calculated in the split band limit for no correlation between diagonal and off-diagonal randomness and compared with the ordered and SS-CPA density of states.

1. Introduction

Ever since Soven[1]) introduced the single-site coherent potential approximation (SS-CPA) for the study of disordered systems, many papers[2]) have applied the approximation to the calculation of the properties of disordered solids. The SS-CPA is applicable only to the case of diagonal randomness, and these results have been criticized by Stern[3]).

Previous attempts have been made to extend the CPA to off-diagonal randomness[4]). A self-consistent extension is discussed here.

2. Theory

The disordered binary alloy A_xB_{1-x} is characterized by the Hamiltonian

$$H = \Sigma_l |l\rangle \varepsilon_l \langle l| + \Sigma_{l \neq m} |l\rangle W_{lm} \langle m|, \qquad (1)$$

* Supported in part by NASA grant #NGR-09-005-072.
** Supported in part by Naval Ordnance Systems Command, Contract #NOw-62-0604-c, Task A13B, and NASA grant #NGR-21-009-033.
† Present address: Harry Diamond Laboratories, Washington, D.C. 20438, U.S.A.

where the atomic energy, ε_l, can take the value ε_A or ε_B and the off-diagonal matrix element, W_{lm}, can assume the values W_{AA}, W_{AB}, or W_{BB}.

In the spirit of the SS-CPA, a configuration-independent Hamiltonian is introduced by

$$H_0 = \Sigma_l |l\rangle \Sigma_0 \langle l| + \Sigma_{l \neq m} |l\rangle \Sigma_1 \langle m|, \tag{2}$$

where $\Sigma_0 = \Sigma_{ll}$ and $\Sigma_1 = \Sigma_{lm}$ are the diagonal and off-diagonal coherent potentials, respectively. The index m in each of the Hamiltonians will be restricted to the first nearest neighbor of l. The Green's functions satisfy the equations $(E-H)\,G = 1$ and $(E-H_0)\,G_0 = 1$ and are related by $G = G_0 + G_0 \times \times TG_0$, where $\Gamma = H - H_0$ and the scattering T-matrix is given by $T = \Gamma + \Gamma G_0 T$. The self-consistency criterion, $\langle G \rangle = G_0$ yields $\langle T \rangle = 0$, where the angular brackets indicate a configurational average.

Since the operator Γ consists of diagonal and off-diagonal components, it is convenient to introduce two T-matrix equations corresponding to the scattering from the two components, i.e.,

$$T_i = \Gamma_i + \Gamma_i G_0 T_i, \quad i = 1,2, \tag{3}$$

where

$$\Gamma_1 = \Sigma_l \Gamma(l) = \Sigma_l |l\rangle (\varepsilon_l - \Sigma_0) \langle l|, \tag{4}$$

and

$$\Gamma_2 = \Sigma_{l \neq m} \Gamma(l, m) = \Sigma_{l \neq m} |l\rangle (W_{lm} - \Sigma_1) \langle m|. \tag{5}$$

The total T-matrix can then be written as

$$T = T_1 + T_2 + (T_1 G_0 B V + T_2 G_0 A U + A U + B V), \tag{6}$$

where

$$A = T_1 G_0 T_2, \tag{7}$$

$$B = T_2 G_0 T_1, \tag{8}$$

$$U = (1 - G_0 A)^{-1}, \tag{9}$$

$$V = (1 - G_0 B)^{-1}. \tag{10}$$

The first two terms in eq. (6) represent independent scattering from Γ_1 and Γ_2. while the last terms enclosed by parenthesis represent the correlated scattering of Γ_1 and Γ_2.

The two operators, Γ_1 and Γ_2, are written as sums over single entities, i.e., over single site and pair operators as in eqs. (4) and (5). Then

$$T_1 = \Sigma_l \Gamma(l) + \Sigma_{l_1, l_2} \Gamma(l_1)\, G_0\, \Gamma(l_2) + \cdots \tag{11}$$

This can be written in terms of the single-site t-matrix

$$t(l) = \Gamma(l) + \Gamma(l)\, G_0\, t(l),$$

as

$$T_1 = \Sigma_l t(l) + \Sigma_{l_1 \neq l_2} t(l_1)\, G_0\, t(l_2) + \cdots. \tag{12}$$

Since there are two coherent potentials, only two matrix elements of T are needed, viz., T_{ll} and T_{lm}, l and m being first nearest neighbor pairs. Simultaneously, intermediate states appearing in these matrix elements are restricted to first nearest neighbor pairs. A set of terms consistent with this pair approximation must be extracted from the l-l and l-m matrix elements of eq. (12). Hence, scatterings from l and its nearest neighbor site must be considered. The diagonal elements of $\langle T_1 \rangle$ in the pair approximation are

$$\langle (T_1)_{ll} \rangle = \langle t_l \rangle + Z \langle t_l^2 g_1^2 t_m / (1 - g_1^2 t_l t_m) \rangle , \tag{13}$$

where $t_l = (l|t(l)|l)$, $g_1 = (l|G_0|m)$ and Z = number of first nearest neighbors. Eq. (13) represents the SS-CPA t-matrix vertex corrected for scattering from its first nearest neighbor.

It can be shown that the off-diagonal matrix elements of $\langle T_1 \rangle$ are

$$\langle (T_1)_{lm} \rangle = Z \langle g_0 t_l t_m / (1 - g_1^2 t_l t_m) \rangle . \tag{14}$$

If scattering off the nearest neighbor atom is neglected, i.e., $g_1 = 0$, then $\langle (T_1)_{ll} \rangle = \langle t_l \rangle$ and $\langle (T_1)_{lm} \rangle = 0$ which is the SS-CPA result.

Now, if $\alpha = (l, m)$ designates an (l, m) pair, then

$$T_2 = \Sigma_\alpha \Gamma(\alpha) + \Sigma_{\alpha,\beta} \Gamma(\alpha) G_0 \Gamma(\beta) + \cdots , \tag{15}$$

which can be written in terms of a pair-site t-matrix, $t(\alpha) = \Gamma(\alpha) + \Gamma(\alpha) G_0 \times$ $\times t(\alpha)$, as

$$T_2 = \Sigma_\alpha t(\alpha) + \Sigma_{\alpha \neq \beta} t(\alpha) G_0 t(\beta) + \cdots . \tag{16}$$

Then in the pair approximation

$$\langle (T_2)_{ll} \rangle = Z \langle t_{ll} \rangle , \tag{17}$$

and

$$\langle (T_2)_{lm} \rangle = Z \langle t_{lm} \rangle , \tag{18}$$

where $t_{ll} = (l|t_\alpha|l)$ and $t_{lm} = (l|t_\alpha|_m)$. The matrix elements, t_{ll} and t_{lm}, are found by taking the diagonal and off-diagonal matrix elements of the pair-site t-matrix and solving the resultant set of coupled equations. Then

$$t_{ll} = \Gamma_{ml}^2 g_0 / ((1 - \Gamma_{ml} g_1)^2 - \Gamma_{ml}^2 g_0) , \tag{19}$$

and

$$t_{lm} = \Gamma_{lm} (1 - \Gamma_{lm} g_1) / ((1 - \Gamma_{ml} g_1)^2 - \Gamma_{ml}^2 g_0) . \tag{20}$$

Given the matrix elements of T_1 and T_2 are known, the diagonal and off-diagonal contributions to the correlation terms in eq. (6) can be found. The self-consistency condition, $\langle T_{ll} \rangle = \langle T_{lm} \rangle = 0$, results in two non-linear equations for two unknowns, Σ_0 and Σ_1.

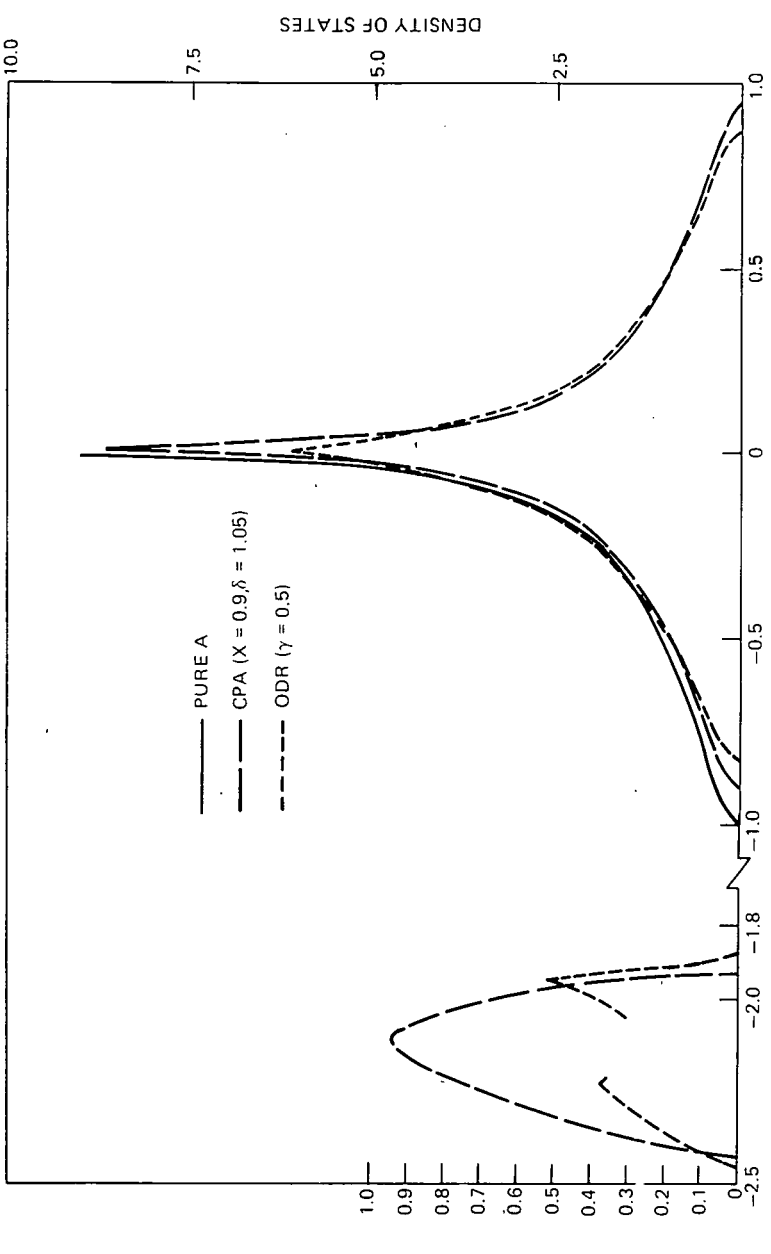

Fig. 1. The density of states (in units of $\pi\ Z\ W_{AA}$) versus reduced energy $(E-\varepsilon_A)/Z\ W_{AA}$ for a bcc lattice. $W_{BB}=W_{AA}$, $W_{AB}=\gamma W_{AA}$, X = concentration of A atoms and $\delta=(\varepsilon_A-\varepsilon_B)/Z\ W_{AA}$, where $\varepsilon_B=-\varepsilon_A$. The scale on the right is for the

3. Results

These two equations without correlation were solved iteratively for a bcc lattice. The density of states is shown in fig. 1 and compared with the SS-CPA. The incompleted part of the curve in the impurity band results from the lack of convergence in the solutions. The novel feature is the appearance of structure in the impurity band which is absent in the SS-CPA. Further details and discussions will be published elsewhere.

References

1) P. Soven, Phys. Rev. **156** (1967) 809.
2) See refs. 3–13, quoted in ref. 3.
3) E. A. Stern, Phys. Rev. Letters **26** (1971) 1630.
4) K. Moorjani, T. Tanaka and S. M. Bose, Advan. Phys., to be published;
J. A. Blackman, N. F. Berk and D. M. Esterling, to be published;
E-N. Foo and M. Ausloos, J. Non-Crystalline Solids **8–10** (1972) 134.

Coherent Potential Theory of a Random Binary Alloy; Effects of Scattering from Two-Sites Clusters and Off-Diagonal Randomness

KISHIN MOORJANI*
Applied Physics Laboratory, The Johns Hopkins University,
Silver Spring, Maryland 20910

and

TOMOYASU TANAKA†
Department of Physics, The Catholic University of America
Washington, D. C. 20017

and

MARTIN M. SOKOLOSKI†
Harry Diamond Laboratories, Washington, D. C. 20438

and

SHYAMALENDU M. BOSE†
Department of Physics, Drexel University
Philadelphia, Pennsylvania 19104

*Supported in part by Naval Ordnance Systems Command, Contract N00017-72-C-4401, Task A13B, and NASA Grant NGR-21-009-033.

†Supported in part by NASA Grant NGR-09-005-072.

A one-band model of a random binary alloy A_xB_{1-x} is analyzed in terms of a two-sites coherent potential approximation. In the tight-binding Hamiltonian, the off-diagonal randomness is introduced via the composition dependent hopping energies between nearest neighbor sites. The inclusion of the off-diagonal randomness correlates the scattering from a given site to that from its nearest neighbors. Such a correlation is incorporated in the handling of diagonal randomness (arising from the composition dependence of the atomic potentials) by treating the diagonal randomness in the pair approximation. The theory leads to the wave-vector-dependent coherent potentials and previous approximations used in this problem are easily obtained in appropriate limits. The numerical results for the electron density of states are presented for a number of different alloys and compared with earlier calculations. For the case of diagonal randomness only, the present theory results in the appearance of structure in the density of states of the minority component band. This is in contrast to the results obtained from the single-site coherent potential approximation, but in agreement with the recent work of Schwartz and Siggia. The presence of the off-diagonal randomness leads to further structure in the density of states.

I. INTRODUCTION

The coherent potential approach, based on the multiple scattering formalism of Lax (1951), has proved to be a useful method for the investigation of disordered alloys. A simple and elegant version of this approach, referred to as the single-site coherent potential approximation (SS-CPA) (Soven 1967, Velicky et al. 1968) has been fruitfully applied to a random binary alloy A_xB_{1-x} in which disorder arises only due to the difference between the atomic potentials of the two components of the alloy. The hopping integrals in the tight-binding Hamiltonian are assumed to be independent of the composition of the alloy and hence are translationally invariant. Thus, only the diagonal part of the Hamiltonian is assumed to be random.

The SS-CPA has been elucidated (Velicky et al. 1968) and applied to various semiconducting and metallic alloys (Stroud and Ehrenreich 1970, Levin and Ehrenreich 1971, Economou et al. 1970). It has been extended to the calculation of transport coefficients (Velicky 1969, Levin et al. 1970) and optical absorption (Velicky and Levin 1970) and its equivalence to previous approaches based on atomic picture (Matsubara and Toyozawa 1961, Yonezawa and Matsubara 1966, Matsubara and Kaneyoshi 1966) (in contrast to the CPA, which is based on strating from an averaged crystalline solid) has been demonstrated (Leath 1970, Ducastelle 1971).

However, a recent criticism of the SS-CPA is worth noting. As Stern (1971) has pointed out, the numerical work based on the SS-CPA has very little applicability to real alloys. The essential weakness of the model lies in the perturbation (introduced by substituting a B-atom for an A-atom) being localized at each atom. Consequently, it is imperative that an extension of the SS-CPA to include non-localized perturbations should be formulated to discuss the electronic properties of disordered binary alloys. One such extension is the subject of the present paper.

We consider a tight-binding Hamiltonian $\mathcal{H}$ of a random binary alloy in which the atomic potentials as well as hopping integrals are assumed to be dependent on the composition of the alloy*. In the spirit of the coherent potential theory, an effective Hamiltonian $\mathcal{H}_0$ is introduced via the diagonal coherent potential Σ_0 and the off-diagonal coherent potential Σ_1. The latter quantity is, however, restricted to a pair of nearest neighbor sites. This is an important assumption and essential to keeping the formalism tractable and the numerical work manageable. With this assumption, the diagonal and the off-diagonal randomness (ODR) can be treated separately. The presence of ODR necessarily correlates a given site ℓ with any of its Z nearest neighbors. Consequently, such a correlation should be included in calculating the effects of diagonal randomness. This requires

* Some aspects of the present work have been previously reported by Moorjani et al. (1971) and Tanaka et al. (1972).

that the diagonal randomness should be treated in the pair approximation within the framework of the coherent potential theory.

The pair scattering, in the absence of ODR, has been discussed in the literature by various authors (Aiyer et al. 1969, Freed and Cohen 1971, Cyrot-Lackmann and Ducastelle 1971, Nickel and Krumhansl 1971, Schwartz and Siggia 1972, Leath 1972, Cyrot-Lackmann and Cyrot 1972, Schwartz and Ehrenreich 1972). Leath (1972) has pointed out the differences which exist amongst various results. The main reason for these differences is discussed in Sections II and III which contain the general formulation of the problem. The detailed calculations are carried out in the two appendices. Section IV contains the main results of this work and its relationship to previous approximations. The numerical results are discussed and compared with earlier calculations in Section V, and the conclusions are presented in the final section.

II. FORMALISM

We consider the tight-binding model of a random binary alloy A_xB_{1-x} which is characterized by the Hamiltonian,

$$\mathcal{H} = \sum_{\ell} |\ell\rangle \epsilon_{\ell} \langle \ell| + \sum_{\ell \neq m} |\ell\rangle W_{\ell m} \langle m| \qquad (1).$$

The summation in the first term extends over all atomic sites while that in the second is restricted to the nearest neighbors only. The atomic energies ϵ_{ℓ} as well as the overlap integrals $W_{\ell m}$ are taken to be composition dependent; ϵ_{ℓ} assumes the values ϵ_A or ϵ_B depending on whether the ℓ^{th} site is occupied by an A-atom or a B-atom and $W_{\ell m}$ takes the values W_{AA}, W_{BB} or W_{AB} $(=W_{BA})$.

The Green's function corresponding to the above equation is defined by the relation,

$$G(E) = \frac{1}{E-\mathcal{H}} \qquad (2),$$

where E is the complex energy.

In the general spirit of the coherent potential theory, we introduce an effective medium for the motion of an electron, and assume that the effective Hamiltonian can be written as,

$$\mathcal{H}_o = \sum_{\ell} |\ell\rangle \Sigma_o \langle \ell| + \sum_{\ell \neq m} |\ell\rangle \Sigma_1 \langle m| \qquad (3),$$

where the summation conventions are the same as in Eq.(1). The effective or coherent potentials Σ_o $(=\Sigma_{\ell\ell})$ and

$\Sigma_1 (=\Sigma_{\ell m})$ are as yet unknown, to be determined from an appropriate self-consistent condition. We assume that the largest contribution to the off-diagonal coherent potential comes from the nearest neighbor sites; an assumption which is essential for keeping the numerical work within reasonable bounds.

The static properties of the system are determined from the configurational average of the Green's function [Eq.(2)] over all possible configurations of the random alloy. The electron density of states, for example, is given by the well-known relationship,

$$\rho(E) = -\frac{1}{\pi} \text{ Im Trace } \langle G(E) \rangle \qquad (4),$$

where the angular brackets denote the configurational average. When the configurationally averaged medium is taken to be the effective medium defined by Eq.(3), then one obtains the identity,

$$\langle G(E) \rangle = G_o(E) = \frac{1}{E - \mathcal{K}_o} \qquad (5).$$

The exact $G(E)$ [Eq.(2)] is then related to $G_o(E)$ by the relationship

$$G = G_o + G_o T G_o \qquad (6),$$

where the T-matrix is defined by,

$$T = \Gamma(1 + G_o T) \qquad (7),$$

with $\Gamma = \mathcal{H} - \mathcal{H}_o$ (8),

If one now takes the configuration average of Eq.(6), one obtains

$$\langle T \rangle = 0 \qquad (9),$$

a condition which can be used to determine the coherent potentials Σ_o and Σ_1. It should be noted that Eq.(9) represents a general exact condition. The various approximations become clearer if the physical contents of the above mathematical formulation are made a bit more transparent.

The actual potentials ϵ_ℓ and $W_{\ell m}$ which an electron experiences during its motion in a given disordered alloy are replaced in the effective medium by the unknown quantities Σ_o and Σ_1. The multiple scattering of the electron are described by the T-matrix (Eq.7) and the unknown potentials determined from the condition that there be no further scattering in the effective medium. Since there are only two unknowns, we need just two equations; these are obtained by taking the diagonal and the off-diagonal matrix elements between nearest neighbors of Eq.(9). One thus obtains

$$\langle T \rangle_{\ell\ell} = 0 \qquad (10\text{-a})$$

$$\langle T \rangle_{\ell m} = 0 \qquad (10\text{-b}),$$

At this point, a digression is essential to point out the relationship of the above formalism with the SS-CPA, and more important to point out the subtle but significant difference between our approach and that of Foo, et al. (1971). In SS-CPA one concentrates on a single effective atom and requires that there be no further scattering from it. The exact self-consistent condition (Eq.9) is thus replaced by the one which requires that the configurational average of the atomic t-matrix must vanish; this single equation being adequate to determine the single unknown Σ_o. Foo, et al. (1971)carry out a straightforward extension of the SS-CPA, replacing a single atom by a pair of nearest neighbor atoms requiring that there be no further scattering from the two-atom cluster in the effective medium. This clearly does not treat the Z nearest neighbors of a given atom on the same footing; a drawback realized but not accounted for by Foo, et al.(1971). It is not correct, as they state, that such a difficulty is an essential element of any self-consistent treatment of pair-scattering. As discussed below, the difficulty can indeed be removed and has the expected effect of multiplying all scattering matrix elements from a pair of nearest neighbors by a factor of Z. To illustrate this point, let us decompose the T-matrix as,

$$T = \sum_{\ell} T(\ell) + \sum_{\ell \neq m} T(\ell,m) + \sum_{n \neq (\ell,m)} T(\ell,m,n) + \ldots \quad (11),$$

where, $T(\ell)$ is an operator which accounts for scattering from the ℓ^{th} site, $T(\ell,m)$ from all pairs of sites, $T(\ell,m,n)$ from all three-site clusters and so on. The first summation is over all sites, the second over all pairs and so on. In the approximation, where the effects of three atoms and higher order clusters are neglected and the two-site clusters are restricted only to the nearest neighbors, Eq.(11) can be truncated and written as,

$$T = \sum_{\ell} T(\ell) + \sum_{m \neq \ell} T(\ell,m) \quad (12),$$

where the second summation is only over the nearest neighbors. Taking the configurational average, we obtain

$$\langle T \rangle = \sum_{\ell} \langle T(\ell) \rangle + \sum_{m \neq \ell} \langle T(\ell,m) \rangle \quad (13).$$

The matrix elements in Wannier representation are therefore given by,

$$\langle T \rangle_{\ell\ell} = \langle T(\ell) \rangle_{\ell\ell} + \sum_{m \neq \ell} \langle T(\ell,m) \rangle_{\ell\ell} \quad (14\text{-a})$$

and

$$\langle T \rangle_{\ell m} = \sum_{m \neq \ell} \langle T(\ell,m) \rangle_{\ell m} \quad (14\text{-b})$$

Combining $Eq^{ns}(14)$ with $Eq^{ns}(10)$, and taking advantage of the fact that configurationally averaged quantities are translationally invariant, one finally obtains,

$$\langle T(\ell)\rangle_{\ell\ell} + Z\langle T(\ell,m)\rangle_{\ell\ell} = 0 \qquad (15\text{-a})$$

and

$$Z\langle T(\ell,m)\rangle_{\ell m} = 0 \qquad (15\text{-b})$$

Foo, et al. (1971) leave out the factor Z in the above equations which as seen is important only in Eq.(15-a). In relation to the work of various authors on pair scattering, this point is further discussed in the next section where we obtain explicit expressions for the diagonal and the off-diagonal matrix elements of the T-matrix.

III. MATRIX ELEMENTS OF THE T-MATRIX

The form of the actual and the effective Hamiltonians [Eq^{ns}(1) and (3)] suggest that the perturbation Hamiltonian Γ (Eq.8) can be conveniently separated into the diagonal and the off-diagonal parts, as

$$\Gamma = \Gamma^{(1)} + \Gamma^{(2)} \tag{16}$$

where,

$$\Gamma^{(1)} = \sum_{\ell} \Gamma^{(1)}(\ell) = \sum_{\ell} |\ell\rangle (\epsilon_{\ell} - \Sigma_{o}) \langle \ell| \tag{17-a}$$

and

$$\Gamma^{(2)} = \sum_{(\alpha)} \Gamma^{(2)}(\alpha) = \sum_{m \neq \ell} |\ell\rangle (W_{\ell m} - \Sigma_{1}) \langle m| \tag{17-b}$$

In the last equation, α denotes a pair of nearest neighbor sites (ℓ,m).

Corresponding to $\Gamma^{(1)}$ and $\Gamma^{(2)}$, one can now define the T-matrices via the equation

$$T^{(i)} = \Gamma^{(i)}\left[1 + G_{o} T^{(i)}\right] \quad (i = 1,2) \tag{18}.$$

$T^{(1)}$ and $T^{(2)}$ describe the multiple scattering of an electron from the diagonal and the off-diagonal perturbation Hamiltonians respectively. The total T-matrix (Eq.7)

can then be written in terms of $T^{(1)}$ and $T^{(2)}$ as,

$$T = \left[T^{(1)} + R\right]Q + \left[T^{(2)} + S\right]P \tag{19}$$

where,

$$P = \left[1 - G_o S\right]^{-1} \tag{20-a},$$

$$Q = \left[1 - G_o R\right]^{-1} \tag{20-b},$$

$$R = T^{(2)} G_o T^{(1)} \tag{20-c},$$

and,

$$S = T^{(1)} G_o T^{(2)} \tag{20-d}.$$

It should be noticed that Eq.(19) represents an exact expression for T in the nearest neighbor pair approximation and includes the sum of the scatterings from $\Gamma^{(1)}$ and $\Gamma^{(2)}$ plus all the correlations where an electron is alternatively scattered any number of times by $\Gamma^{(1)}$ and $\Gamma^{(2)}$. To determine the matrix elements of T, one needs to calculate the matrix elements of $T^{(1)}$ and $T^{(2)}$ only since P, Q, R, and S are expressed in terms of these quantities (Eq.20).

To evaluate the matrix elements of $T^{(2)}$, we combine Eqns(17-b) and (18) to write,

$$T^{(2)} = \sum_{\alpha} \Gamma^{(2)}(\alpha) + \sum_{\alpha,\beta} \Gamma^{(2)}(\alpha) G_o \Gamma^{(2)}(\beta) + \ldots. \tag{21},$$

which can be rewritten in terms of a pair-site t-matrix,

$$t(\alpha) = \Gamma^{(2)}(\alpha)\left[1 + G_o\, t(\alpha)\right] \tag{22},$$

as,

$$T^{(2)} = \sum_{\alpha} t(\alpha) + \sum_{\alpha\neq\beta} t(\alpha) G_o\, t(\beta) + \ldots. \tag{23}.$$

Thus in the nearest-neighbor pair approximation,

$$\langle T^{(2)}\rangle_{\ell\ell} = Z\,\langle t_{\ell\ell}\rangle \tag{24},$$

and,

$$\langle T^{(2)}\rangle_{\ell m} = Z\,\langle t_{\ell m}\rangle \tag{25},$$

where,

$$t_{\ell\ell} = \langle \ell|\, t(\alpha)\,|\ell\rangle \quad \text{and} \quad t_{\ell m} = \langle \ell|\, t(\alpha)\,|m\rangle \tag{26}.$$

The matrix elements $t_{\ell\ell}$ and $t_{\ell m}$ are obtained from Eq.(22) and solving a set of coupled equations to yield,

$$t_{\ell\ell} = \Gamma^2_{m\ell} g_o \Big/ \left[(1 - \Gamma_{m\ell} g_1)^2 - \Gamma^2_{m\ell} g_o^2\right] \tag{27}$$

and,

$$t_{\ell m} = \Gamma_{\ell m}(1 - \Gamma_{\ell m} g_1) \Big/ \left[(1 - \Gamma_{m\ell} g_1)^2 - \Gamma^2_{m\ell} g_o^2\right] \tag{28}.$$

In Eq^{ns}(27) and (28), $\Gamma_{m\ell} = \Gamma_{\ell m} = W_{\ell m} - \Sigma_1$ and the diagonal and the off-diagonal matrix elements of G_o are given by,

$$g_o = \langle \ell | G_o | \ell \rangle \quad \text{and} \quad g_1 = \langle \ell | G_o | m \rangle \qquad (29).$$

The presence of off-diagonal randomness, as seen in Eq^{ns}(24-28), correlates the ℓ^{th} site to its nearest neighbor sites via $\Gamma_{\ell m}$. This further manifests itself in the appearance of g_1, which determines the propagation of a single particle state from a given site to any of its Z nearest neighbors. To be consistent this correlation should also be included in the diagonal randomness. This requires that $T^{(1)}$ be treated in the pair approximation, in contrast to the recent work of Blackman, et al. (1971).

The pair scattering treatment of $T^{(1)}$ has been carried out by various authors in the literature. However, as Leath (1972) hasrecently pointed out, some differences among various results still exist. A simple diagrammatic procedure outlined below leads to the expression first reported by Cyrot-Lackmann and Ducastelle (1971).

Combining Eq^{ns}(17-a) and (18), $T^{(1)}$ can be written as,

$$T^{(1)} = \sum_{\ell} \Gamma^{(1)}(\ell) + \sum_{\ell_1, \ell_2} \Gamma^{(1)}(\ell_1) G_o \Gamma^{(1)}(\ell_2) + \ldots . \qquad (30),$$

which in turn can be written in terms of the single-site t-matrix,

$$t(\ell) = \Gamma^{(1)}(\ell)\left[1 + G_o t(\ell)\right] \qquad (31),$$

as,

$$T^{(1)} = \sum_{\ell} t(\ell) + \sum_{\ell_1 \neq \ell_2} t(\ell_1) G_0 t(\ell_2)$$

$$+ \sum_{\ell_1 \neq \ell_2 \neq \ell_3} t(\ell_1) G_0 t(\ell_2) G_0 t(\ell_3) + \ldots . \qquad (32).$$

The summation convention in the last equation implies that no two successive indices can be equal to each other. For example, in the third term $\ell_1 \neq \ell_2$ and $\ell_2 \neq \ell_3$ but ℓ_1 can be equal to ℓ_3. Diagrammatically, Eq.(32) can be written as shown in Fig.(1). If one now neglects the effects of three-sites and higher order clusters, then one needs to keep only those diagrams [Fig.(1)] which involve one and two distinct sites. Thus, in the pair approximation, some of the diagrams which contribute to $T^{(1)}$ are those shown in Fig. (2). Summing this series of diagrams and taking the configurational average, one obtains,

$$\langle T^{(1)} \rangle = \sum_{\ell} \langle t(\ell) \rangle + \sum_{\ell_1 \neq \ell_2} \langle t(\ell_1) G_0 t(\ell_2) G_0 t(\ell_1)$$

$$\left[1 - G_0 t(\ell_2) G_0 t(\ell_1)\right]^{-1} + t(\ell_1) G_0 t(\ell_2)$$

$$\left[1 - G_0 t(\ell_1) G_0 t(\ell_2)\right]^{-1} \rangle \qquad (33).$$

Next, we restrict ℓ_2 to be the nearest neighbors of ℓ_1, and take diagonal and nearest neighbor off-diagonal matrix

elements in Wannier representation. Using the isotropy and the translational invariance of the lattice we find

$$\langle T^{(1)} \rangle_{\text{diag}} = \sum_{\ell} \langle T^{(1)} \rangle_{\ell\ell} \tag{34-a}$$

where,

$$\langle T^{(1)} \rangle_{\ell\ell} = \langle t_{\ell} \rangle + Z \langle t_{\ell}^2 t_m g_1^2 / (1 - t_{\ell} t_m g_1^2 \rangle \tag{34-b}$$

and,

$$\langle T^{(1)} \rangle_{\text{off-diag}} = \sum_{(\ell,m)} \langle T^{(1)} \rangle_{\ell m} \tag{35-a}$$

with

$$\langle T^{(1)} \rangle_{\ell m} = Z \langle t_{\ell} t_m g_1 / (1 - t_{\ell} t_m g_1^2) \rangle \tag{35-b}$$

where m is one of the nearest neighbors of ℓ and,

$$t_{\ell} = \langle \ell | t(\ell) | \ell \rangle = \frac{\epsilon_{\ell} - \Sigma_o}{1 - g_o (\epsilon_{\ell} - \Sigma_o)} \tag{36}.$$

The last equality follows from Eq.(31) combined with Eq. (17-a).

The expressions (34-b) and (35-b) are easily shown to be identical to the results obtained by Cyrot-Lackmann and Ducastelle (1971) but differ from the treatments of other

authors (Nickel and Krumhansl 1971, Leath 1972, Foo et al. 1971) by the appearance of Z the number of nearest neighbors. It should also be pointed out that the recent criticism by Cyrot-Lackmann and Cyrot (1972) of their earlier formulation (Cyrot-Lackmann and Ducastelle 1971) is valid only if one considers atoms which are not nearest neighbors of each other.

It remains to evaluate the matrix elements of P, Q, R and S [Eq.(20)] and take the configurational averages. This part of the calculation is carried out in the two appendices and the results are discussed in the next section.

IV. RESULTS

As shown in Appendix II, we obtain two equations from the two self-consistent relations [Eq^{ns}(10-a) and (10-b)] which can be written as the coupled equation for the two coherent potentials. The resulting equations, obtained from Eq.(A-23) and the combination of Eq.(A-29) with Eq. (A-20), respectively are

$$\Sigma_o = U_o - (\epsilon_A - \Sigma_o) g_o (\epsilon_B - \Sigma_o) + Z\left[1 - (\epsilon_A - \Sigma_o) g_o\right] \left[1 - (\epsilon_B - \Sigma_o) g_o\right] F_o \quad (37)$$

and,

$$\Sigma_1 = U_1 + \xi + \left[1 - g_1 \Gamma(x,x)\right]\left[1 - g_1 \Gamma(x,y)\right] \left[1 - g_1 \Gamma(y,y)\right] \left(F_1 + F_2\right) \quad (38)$$

The quantities F_o, F_1, F_2, ξ and Γ's are defined by Eq^{ns} (A-17), (A-27),(A-21), (A-30) and (A-19-f) respectively. U_o and U_1 are the potentials in the virtual crystal approximation given by,

$$U_o = x\epsilon_A + y\epsilon_B \quad (39)$$

and

$$U_1 = x^2 W_{AA} + 2xyW_{AB} + y^2 W_{BB} \quad (40)$$

One notices that previously used approximations are contained in Eq^{ns}(37) and (38). Thus the first terms in these equations represent the virtual crystal approximation and the first two terms in Eq.(37) reproduce the result obtained in the SS-CPA. The rest of the terms are the corrections due to the inclusion of pair-scattering and off-diagonal randomness in the present analysis.

To solve Eq^{ns}(37) and (38), it is convenient to transform them in dimensionless form. We shall therefore refer all quantities to ZW_{AA}, the half-bandwidth of the pure A-lattice. Furthermore, we assume that $\epsilon_B = -\epsilon_A$, and obtain

$$\sigma_o = \frac{\Sigma_o}{ZW_{AA}} = (x - y)\,\delta + (\delta^2 - \sigma_o^2)P_o + Z\left[1 - (\delta - \sigma_o)P_o\right]\left[1 + (\delta + \sigma_o)P_o\right]f_o \qquad (41)$$

and,

$$\sigma_1 = \frac{\Sigma_1}{ZW_{AA}} = W_1 + \xi' + (1 - \Gamma_{AA}\,P_1)(1 - \Gamma_{AB}\,P_1)(1 - \Gamma_{BB}P_1)(f_1 + f_2) \qquad (42)$$

where,

$$f_i = F_i/ZW_{AA}, \quad \xi' = \xi/ZW_{AA} \qquad (43)$$

$$P_o = ZW_{AA}g_o \qquad (44)$$

$$P_1 = ZW_{AA}g_1 \tag{45}$$

$$\delta = \frac{\epsilon_A - \epsilon_B}{2ZW_{AA}} = \epsilon_A/ZW_{AA} \tag{46}$$

$$W_1 = \frac{1}{Z}\,(x^2 + 2\gamma xy + \beta y^2) \tag{47}$$

and,

$$\Gamma_{AA} = \frac{\Gamma(x,x)}{ZW_{AA}} = \frac{1}{Z} - \sigma_1$$

$$\Gamma_{AB} = \Gamma_{BA} = \frac{\Gamma(x,y)}{ZW_{AA}} = \frac{\gamma}{Z} - \sigma_1$$

$$\Gamma_{BB} = \frac{\Gamma(y,y)}{ZW_{AA}} = \frac{\beta}{Z} - \sigma_1 \tag{48}$$

The last equations result from defining the bandwidths of A-B and B-B lattice in terms of the A-A lattice; $W_{AB} = \gamma W_{AA}$ and $W_{BB} = \beta W_{AA}$.

Before representing the numerical results, let us note that g_o and g_1 (Eq.28) can be written in k-representation as,

$$g_o = \frac{1}{N}\sum_k \frac{1}{E - \Sigma_o - \Sigma_1\gamma(k)} \tag{49}$$

and

$$g_1 = \frac{1}{N}\sum_k \frac{e^{ik.(\ell - m)}}{E - \Sigma_o - \Sigma_1\gamma(k)} \tag{50}$$

where $\gamma(k) = \sum_{\Delta} e^{ik.\Delta}$ is the structure factor, Δ being the nearest-neighbor vector. In Eq.(50), ℓ and m are nearest neighbors and therefore,

$$g_1 = \alpha g_o - \frac{1}{Z\Sigma_1} \tag{51}$$

where the dimensionless parameter α is defined by,

$$\alpha = \frac{E - \Sigma_o}{Z\Sigma_1} = \frac{E' - \sigma_o}{Z\sigma_1}, \quad (E' = E/ZW_{AA}) \tag{52}$$

The dimensionless quantities P_o and P_1 [Eq^{ns}(44) and (45)] are therefore given by

$$P_o = \frac{1}{Z\sigma_1} \frac{1}{N} \sum_k \frac{1}{\alpha - Z^{-1}\gamma(k)} \tag{53},$$

and

$$P_1 = \alpha P_o - \frac{1}{Z\sigma_1} \tag{54}.$$

The quantity of interest is the electronic density of states (Eq.4) which can be expressed as,

$$\rho(E) = -\frac{1}{\pi} \text{Im} \sum_{\ell} \langle \ell | G_o | \ell \rangle = -\frac{N}{\pi} \text{Im} g_o$$

or

$$\rho'(E) = ZW_{AA} \left(\frac{\rho(E)}{N}\right) = -\frac{1}{\pi} \text{Im} P_o \tag{55},$$

$\rho'(E)$ being the density of states/atom expressed in units of half-bandwidth of pure A-lattice.

The two non-linear Eq^{ns} (41) and (42) are now solved iteratively for σ_o and σ_1 as a function of reduced energy E', for given values of x, the concentration of A-atoms; δ, the potential difference between type-A and type-B atoms, and β and γ the relative bandwidth of B-B and A-B lattices respectively with respect to the A-A lattice. The knowledge of the coherent potentials σ_o and σ_1 allows one to compute the imaginary part of P_o and the density of states is obtained from Eq.(55). We have carried out the numerical calculations for a number of different alloys for the body-centered cubic lattice and the results are discussed in the next section.

DISCUSSION

The numerical results for electron density of states/atom [in fact $\pi\rho'$, where ρ' is given by Eq.(55)] as a function of energy for various alloy parameters are presented in this section. The results are illustrated by a number of figures where the normalized Energy E' (Eq. 52) has been shifted by δ so that the band corresponding to the pure A-lattice in these dimensionless units is located at the origin and extends from -1 to $+1$. Throughout the present analysis we have considered the body-centered cubic (BCC) lattice for which the density of states was obtained by using the lattice Green's function recently evaluated by Morita and Horiguchi (1971). The density of states for ordered pure A-BCC lattice is shown in Figure 3 and all effects of disorder are measured with respect to it. Since we have chosen $\epsilon_B = -\epsilon_A$, the effect of substituting B-atoms for A-atoms is expected to be the appearance of a "minority band" located at -2δ, whose width is controlled by the parameters x, β, and γ. Whether any structure due to presence of minority atoms is discernible in the density of states curves, depends as shown below, on the values of these parameters and δ.

The results for the case of a dilute alloy ($x = 0.9$) are presented in Figures 4 and 5 for $\delta = 0.2$

and two different values for the set (β, γ). As shown in the figures, the general effect of disorder is to remove the singularity at the origin in the density of states of the ordered lattice and modify the bandwidth, which is increased for the alloy represented by $(\beta, \gamma) = (1.4, 1.2)$ [Fig. 4] and decreased for the case $(\beta, \gamma) = (0.15, 0.1)$ [Fig. 5]. The density of states in the vicinity of Energy = - 0.4 is increased relative to the ordered lattice showing the presence of the contribution of the minority band. For the larger bandwidth case [Fig. 4] the minority band is relatively flat and no visible structure shows up at Energy = - 0.4. This effect, as expected, is more pronounced for the shorter bandwidth alloy and, as shown in the insert of Figure 5, a shoulder in the density of states is indeed discernable. For a non-dilute alloy, still more pronounced structure would be expected and this is indicated in Figures (6)-(8) for $x = 0.6$, $\delta = 0.2$ and three different bandwidth combinations (β, γ). Note that the peak due to the minority band does not lie exactly at - 0.4 but slowly shifts towards higher energy with increasing values of β and γ, while the main peak shifts towards lower energy. The magnitude of the impurity band peak is lowest for $(\beta, \gamma) = (1.4, 1.2)$ and highest for $(\beta, \gamma) = (0.4, 0.7)$.

In the cases discussed above, we have only considered alloys where the main band and the minority band overlap in energy ($\delta < 1$). In order to compare results with earlier calculations, it is desirable to consider the split-band case ($\delta > 1$) so that the effects of the minority band are clearly separated from that of the main band. Also to facilitate comparison with the SS-CPA, we first consider the alloy with no off-diagonal randomness, i.e. $\beta = \gamma = 1$. For this particular case, the results of Blackman, et al.(1971) reduce to the SS-CPA. This is due to the neglect of pair scattering in their work. Our results (labeled TS-CPA for two sites-CPA) for $x = 0.9$ and $\delta = 1.05$ are presented in Figure 9 and compared with the SS-CPA. In the main band, the differences between the TS-CPA and SS-CPA results are negligible and for clarity only TS-CPA results are shown. However, important and major differences appear in the shape of the minority band (Fig. 9) as obtained in the present work and that calculated from SS-CPA. In the later, one obtains a smoothly varying curve for the density of states in the minority band; a result which originates from the fact that in the SS-CPA, the perturbation is localized at a given site. Consequently the coherent potential is k-independent and is incapable of sampling the lattice. The k-dependent coherent potentials in the present formulation lead to the

appearance of structure on both sides of the minority band (Fig. 9). Following quite a different formulation, Schwartz and Siggia (1972) also find structure in the minority band. Foo, et al. (1971) in their calculations for one-dimensional random chain, have also reported structure in the minority band; however, the location of their minority band is a strong function of the bandwidths β and γ. This incorrect result is due to their special choices of the values of β and γ and is typical of the shape of the density of states of one-dimensional chains.

It is of interest to plot the real and imaginary parts of the coherent potentials σ_0 and σ_1 and compare them with the SS-CPA. This is done in Figures 10-12. As shown in Figures 10 and 11, the inclusion of pair scattering leads to the presence of structure in $\mathrm{Re}\sigma_0$ and $\mathrm{Im}\sigma_0$ which is responsible for the structure in the density of states (Fig. 9). For the off-diagonal coherent potential σ_1 (Fig. 12), the SS-CPA results would be $\mathrm{Im}\sigma_1 = 0$ and $\mathrm{Re}\sigma_1 = 0.125$ over the entire range of the minority band.

Finally, Figure 13 shows the density of states for the case when off-diagonal randomness is present. The presence of the off-diagonal randomness has the advantage of controlling the bandwidth of the minority band by varying the values of β and γ. As shown in Figure 13 for the case $\gamma = 0.5$, further structure appears in the

density of states of the minority band due to the splitting of the central peak. The structure in the absence of the off-diagonal randomness (Fig. 9) has been assigned by Schwartz and Siggia (1972) to the bonding and anti-bonding levels of a molecule embedded in an effective medium. At the time of the present writing, we have not found a satisfactory explanation for the extra structure seen in the presence of the off-diagonal randomness (Fig. 13).

SUMMARY

In this paper, we have extended the single-site coherent potential approximation for random binary alloys to include the effects of the off-diagonal randomness and the pair scattering. The formalism reduces to previous approximations used in this problem in appropriate limits. The numerical results for a number of different alloys are reported and it is shown that the inclusion of pair scattering and off-diagonal randomness leads to the appearance of structure in the density of states of the minority component band.

There remains the problem of investigating the effect of scattering from clusters higher than the two-sites clusters. In principle, this is quite straightforward in the framework of the present theory; however, the numerical work involved is expected to be quite formidable. The theory can also be applied to the calculation of conductivity (Sokoloski et al. 1972) and indeed the study of disordered magnetic systems (Bose et al. 1972). The detailed calculations of such extensions will be reported in the near future.

ACKNOWLEDGEMENTS

We are deeply indebted to Professor T. Morita for sending us the computer program for the evaluation of the density of states for an ordered body-centered cubic lattice. One of us (K. M.) would like to thank S. Favin for his unfailing help with the computer programming.

APPENDIX I

The Matrix Elements

The matrix elements of R [Eq.(20-c)] and S [Eq. (20-d)] between Wannier states on a nearest neighbor pair of sites (ℓ,m) are easily written down in terms of the matrix elements of $T^{(1)}$ and $T^{(2)}$, as

$$\begin{pmatrix} R_{\ell\ell} & R_{\ell m} \\ R_{m\ell} & R_{mm} \end{pmatrix} = \begin{pmatrix} T^{(2)}_{\ell\ell} & T^{(2)}_{\ell m} \\ T^{(2)}_{m\ell} & T^{(2)}_{mm} \end{pmatrix} \begin{pmatrix} g_o & g_1 \\ g_1 & g_o \end{pmatrix} \begin{pmatrix} T^{(1)}_{\ell\ell} & T^{(1)}_{\ell m} \\ T^{(1)}_{m\ell} & T^{(1)}_{mm} \end{pmatrix} \qquad (A\text{-}1),$$

and,

$$\begin{pmatrix} S_{\ell\ell} & S_{\ell m} \\ S_{m\ell} & S_{mm} \end{pmatrix} = \begin{pmatrix} T^{(1)}_{\ell\ell} & T^{(1)}_{\ell m} \\ T^{(1)}_{m\ell} & T^{(1)}_{mm} \end{pmatrix} \begin{pmatrix} g_o & g_1 \\ g_1 & g_o \end{pmatrix} \begin{pmatrix} T^{(2)}_{\ell\ell} & T^{(2)}_{\ell m} \\ T^{(2)}_{m\ell} & T^{(2)}_{mm} \end{pmatrix} \qquad (A\text{-}2).$$

We notice that,

$$S_{\ell\ell} = R_{\ell\ell},\ S_{\ell m} = R_{m\ell},\ S_{m\ell} = R_{\ell m},\ \text{and}\ S_{mm} = R_{mm} \qquad (A\text{-}3)$$

The matrix elements of P and Q can now be obtained by taking the diagonal and the off-diagonal matrix elements of Eq.(20-a) and Eq.(20-b), the resulting expressions are,

$$\begin{pmatrix} Q_{\ell\ell} & Q_{\ell m} \\ Q_{m\ell} & Q_{mm} \end{pmatrix} = \frac{1}{D(\ell,m)} \begin{pmatrix} 1 - g_o R_{mm} - g_1 R_{\ell m} & g_o R_{\ell m} + g_1 R_{mm} \\ g_o R_{m\ell} + g_1 R_{\ell\ell} & 1 - g_o R_{\ell\ell} - g_1 R_{m\ell} \end{pmatrix} \qquad (A\text{-}4)$$

and,

$$\begin{pmatrix} P_{\ell\ell} & P_{\ell m} \\ P_{m\ell} & P_{mm} \end{pmatrix} = \frac{1}{D(\ell,m)} \begin{pmatrix} 1 - g_o S_{mm} - g_1 S_{\ell m} & g_o S_{\ell m} + g_1 S_{mm} \\ g_o S_{m\ell} + g_1 S_{\ell\ell} & 1 - g_o S_{\ell\ell} - g_1 S_{m\ell} \end{pmatrix} \quad (A\text{-}5),$$

where,

$$D(\ell,m) = 1 - g_o (R_{\ell\ell} + R_{mm}) - g_1 (R_{\ell m} + R_{m\ell}) + (g_o^2 - g_1^2)(R_{\ell\ell} R_{mm} - R_{\ell m} R_{m\ell}) \quad (A\text{-}6)$$

The same $D(\ell,m)$ appears in Eq^{ns} (A-4) and (A-5) due to the symmetry relations between R's and S's [Eq.(A-3)].

It is now straightforward to write down the matrix elements of T (Eq.19); we, however, follow a slightly modified approach in order to get the final equations in the form which can be easily compared with previous calculations. To evaluate the diagonal matrix elements $T_{\ell\ell}$, we separate out the single-site and two-site contributions, leading to

$$T_{\ell\ell} = t_\ell + Z\, T_{\ell\ell}(\ell,m) \quad (A\text{-}7)$$

where,

$$T_{\ell\ell}(\ell,m) = (T^{(1)}_{\ell\ell} + R_{\ell\ell}) Q_{\ell\ell} + (T^{(1)}_{\ell m} + R_{\ell m}) Q_{m\ell} + (T^{(2)}_{\ell\ell} + S_{\ell\ell}) P_{\ell\ell} + (T^{(2)}_{\ell m} + S_{\ell m}) P_{m\ell} \quad (A\text{-}8),$$

with

$$T^{(1)}_{\ell\ell} = t^2_\ell t_m g^2_1/(1 - t_\ell t_m g^2_1), \tag{A-9}$$

$$T^{(1)}_{\ell m} = t_\ell t_m g_1/(1 - t_\ell t_m g^2_1), \tag{A-10}$$

$$T^{(2)}_{\ell\ell} = t_{\ell\ell}, \text{ and } T^{(2)}_{\ell m} = t_{\ell m} \tag{A-11}$$

The quantities $t_{\ell\ell}$ and $t_{\ell m}$ in Eq.(A-11) are given by Eq.(27) and Eq.(28) respectively.

To evaluate the off-diagonal matrix elements, we write

$$T_{\ell m} = Z\, T_{\ell m}(\ell, m) \tag{A-12}$$

where

$$\begin{aligned} T_{\ell m}(\ell, m) = {} & T^{(2)}_{\ell m} + \left(T^{(1)}_{\ell\ell} + R_{\ell\ell}\right)Q_{\ell m} + \left(T^{(1)}_{\ell m} + R_{\ell m}\right)Q_{mm} \\ & + \left\{\left[1 + g_o T^{(2)}_{\ell\ell} + g_1 T^{(2)}_{\ell m}\right]S_{\ell\ell} + \left[g_1 T^{(2)}_{\ell\ell} + g_o T^{(2)}_{\ell m}\right]S_{m\ell}\right\}P_{\ell m} \\ & + \left\{\left[1 + g_o T^{(2)}_{\ell\ell} + g_1 T^{(2)}_{\ell m}\right]S_{\ell m} + \left[g_1 T^{(2)}_{\ell\ell} + g_o T^{(2)}_{\ell m}\right]S_{mm}\right\}P_{mm} \end{aligned} \tag{A-13}.$$

The last equation is obtained by rewriting Eq.(19) as,

$$T = T^{(2)} + (T^{(1)} + R)Q + (S + T^{(2)} G_o S)P \tag{A-14}$$

It remains to take configurational average of $T_{\ell\ell}$ and $T_{\ell m}$ and this is carried out in the next appendix.

APPENDIX II

Configurational Averages

Taking the configurational average of Eq.(A-7) and invoking the self-consistency condition [Eq.(10-a)], we obtain

$$\langle t_\ell \rangle = x t_x + y t_y = - Z \langle T_{\ell\ell}(\ell,m) \rangle \qquad \text{(A-15)},$$

where, from Eq.(36),

$$t_{x,y} = \frac{\epsilon_{A,B} - \Sigma_o}{1 - g_o(\epsilon_{A,B} - \Sigma_o)} \qquad \text{(A-16)}.$$

Also,

$$\langle T_{\ell\ell}(\ell,m) \rangle = F_o = \sum_{\substack{I=x,y \\ J=x,y}} IJ \; T_{\ell\ell}(I,J) \qquad \text{(A-17)}$$

with,

$$\begin{aligned} T_{\ell\ell}(I,J) = & \left[T^{(1)}_{\ell\ell}(I,J) + R_{\ell\ell}(I,J)\right] Q_{\ell\ell}(I,J) \\ & + \left[T^{(1)}_{\ell m}(I,J) + R_{\ell m}(I,J)\right] Q_{m\ell}(I,J) \\ & + \left[T^{(2)}_{\ell\ell}(I,J) + S_{\ell\ell}(I,J)\right] P_{\ell\ell}(I,J) \\ & + \left[T^{(2)}_{\ell m}(I,J) + S_{\ell m}(I,J)\right] P_{m\ell}(I,J) \end{aligned} \qquad \text{(A-18)}$$

$R_{\ell\ell}(I,J)$ etc. are obtained from Eq^{ns} (A-1), (A-2), (A-4) and (A-5) and various $T^{(1)}$'s and $T^{(2)}$'s from Eq^{ns} (A-9)-(A-11). One then has,

$$T^{(1)}_{\ell\ell}(I,J) = \frac{t_I^2 t_J g_1^2}{1 - t_I t_J g_1^2} \qquad \text{(A-19a)},$$

$$T^{(1)}_{\ell m}(I,J) = T^{(1)}_{m\ell}(I,J) = \frac{t_I t_J g_1}{1 - t_I t_J g_1^2} \qquad \text{(A-19b)},$$

$$T^{(1)}_{mm}(I,J) = \frac{t_J^2 t_I g_1^2}{1 - t_I t_J g_1^2} \qquad \text{(A-19c)},$$

$$T^{(2)}_{\ell\ell}(I,J) = T^{(2)}_{mm}(I,J) = \frac{\Gamma^2(I,J) g_o}{[1 - \Gamma(I,J) g_1]^2 - \Gamma^2(I,J) g_o^2} \qquad \text{(A-19d)},$$

and

$$T^{(2)}_{\ell m}(I,J) = T^{(2)}_{m\ell}(I,J) = \frac{\Gamma(I,J)[1 - \Gamma(I,J) g_1]}{[1 - \Gamma(I,J) g_1]^2 - \Gamma^2(I,J) g_o^2} \qquad \text{(A-19e)}$$

where

$$\Gamma(I,J) = W(I,J) - \Sigma_1 \,, \quad \left(W(x,x) = W_{AA}, \text{ etc.}\right) \qquad \text{(A-19f)}$$

Finally taking the configurational average of Eq.(A-12) and invoking the self-consistency condition [Eq.(10-b)], we obtain

$$\langle T^{(2)}_{\ell m} \rangle = - \langle F_2 \rangle \qquad \text{(A-20)}$$

where,

$$\langle F_2 \rangle = \sum_{\substack{I=x,y \\ J=x,y}} IJ\ F_2(I,J) \tag{A-21}$$

and $F_2(I,J)$ is obtained from Eq.(A-13),

$$\begin{aligned} F_2(I,J) = &\left[T^{(1)}_{\ell\ell}(I,J) + R_{\ell\ell}(I,J)\right]Q_{\ell m}(I,J) \\ &+ \left[T^{(1)}_{\ell m}(I,J) + R_{\ell m}(I,J)\right]Q_{mm}(I,J) \\ &+ \left\{\left[1 + g_o T^{(2)}_{\ell\ell}(I,J) + g_1 T^{(2)}_{\ell m}(I,J)\right]S_{\ell\ell}(I,J)\right. \\ &\left. + \left[g_1 T^{(2)}_{\ell\ell}(I,J) + g_o T^{(2)}_{\ell m}(I,J)\right]S_{m\ell}(I,J)\right\}P_{\ell m}(I,J) \\ &+ \left\{\left[1 + g_o T^{(2)}_{\ell\ell}(I,J) + g_1 T^{(2)}_{\ell m}(I,J)\right]S_{\ell m}(I,J)\right. \\ &\left. + \left[g_1 T^{(2)}_{\ell\ell}(I,J) + g_o T^{(2)}_{\ell m}(I,J)\right]S_{mm}(I,J)\right\}P_{mm}(I,J) \end{aligned} \tag{A-22}$$

The two equations of interest are Eq.(A-15) and Eq.(A-20) and to put them in reasonable form, we first rewrite Eq.(A-15) as,

$$x\,\frac{\epsilon_A - \Sigma_o}{1 - g_o(\epsilon_A - \Sigma_o)} + y\,\frac{\epsilon_B - \Sigma_o}{1 - g_o(\epsilon_B - \Sigma_o)}$$

$$= -Z\langle T_{\ell\ell}(\ell,m)\rangle = -ZF_o$$

or,

$$\Sigma_o = U_o - (\epsilon_A - \Sigma_o)g_o(\epsilon_B - \Sigma_o) + Z\Big[1 - (\epsilon_A - \Sigma_o)g_o\Big]$$

$$\Big[1 - (\epsilon_B - \Sigma_o)g_o\Big]F_o \qquad \text{(A-23)},$$

which is Eq.(37).

To obtain Eq.(38), we rewrite

$$T^{(2)}_{\ell m} = \frac{\Gamma_{\ell m}}{1 - \Gamma_{\ell m} g_1} + F_1 \qquad \text{(A-24)},$$

where,

$$F_1 = \frac{\Gamma^3_{\ell m} g_o^2}{(1 - \Gamma_{\ell m} g_1)[1 - \Gamma_{\ell m} g_1)^2 - \Gamma^2_{\ell m} g_o^2]} \qquad \text{(A-25)}.$$

Therefore,

$$\langle T^{(2)}_{\ell m} \rangle = x^2 \frac{\Gamma(x,x)}{1 - g_1\Gamma(x,x)} + 2xy \frac{\Gamma(x,y)}{1 - g_1\Gamma(x,y)}$$

$$+ y^2 \frac{\Gamma(y,y)}{1 - g_1\Gamma(y,y)} + \langle F_1 \rangle \qquad \text{(A-26)},$$

where,

$$\langle F_1 \rangle = \sum_{\substack{I=x,y \\ J=x,y}} IJ\ F_1(I,J) \qquad \text{(A-27)},$$

and,

$$F(I,J) = \frac{\Gamma^3(I,J)g_o^2}{[1-\Gamma(I,J)g_1][(1-\Gamma(I,J)g_1)^2-\Gamma^2(I,J)g_o^2]} \qquad \text{(A-28)}.$$

From Eq.(A-26), we have,

$$\langle T^{(2)} \rangle = \frac{U_1 - \Sigma_1 + \xi}{[1-g_1\Gamma(x,x)][1-g_1\Gamma(x,y)][1-g_1\Gamma(y,y)]} + \langle F_1 \rangle \qquad \text{(A-29)},$$

where U_1, the value of the overlap integral in the virtual crystal approximation is given by Eq.(40), and

$$\xi = \Gamma(x,x)\Gamma(x,y)\Gamma(y,y)g_1^2 - (x^2+2xy)\Gamma(x,x)\Gamma(x,y)g_1 - (x^2+y^2)\Gamma(x,x)\Gamma(y,y)g_1 - (y^2+2xy)\Gamma(x,y)\Gamma(y,y)g_1 \qquad \text{(A-30)}.$$

Combining Eq. (A-29) with Eq. (A-20), we finally obtain Eq. (38) for Σ_1.

REFERENCES

Aiyer R N, Elliott R J, Krumhansl J A and Leath P L 1969 Phys. Rev. 181 1006-14

Blackman J A, Esterling D M and Berk N F 1971 Phys. Rev. B4 2412-28

Bose S M, Moorjani K, Tanaka T and Sokoloski M M *Proceedings of International Conference on Amorphous Magnetism, Detroit 1972. To be published in J. Non-Crystalline Solids.*

Cyrot-Lackmann F and Ducastelle F 1971 Phys. Rev. Lett. 27 429-31

Cyrot-Lackmann F and Cyrot M 1972 J. Phys. C. Solid St. Phys. 5 L209-12

Ducastelle F 1971 J. Phys. C. Solid St. Phys. 4 L75-7

Economou E N, Kirkpatrick S, Cohen M H and Eggarter 1970 Phys. Rev. Lett. 25 520-4

Foo E N, Amar H and Ausloos M 1971 Phys. Rev. B4 3350-9

Freed K F and Cohen M H 1971 Phys. Rev. B3 3400-17

Lax M 1951 Rev. Mod. Phys. 23 287-310

Leath P L 1970 Phys Rev. B2 3078-87

Leath P L 1972 Phys Rev. B5 1643-6

Levin K, Velicky B and Ehrenreich H 1970 Phys. Rev. B2 1771-88

Levin K and Ehrenreich H 1971 Phys. Rev. B3 4172-88

Matsubara T and Toyozawa Y 1961 Prog. Theor. Phys. (Kyoto) 26 739-56

Matsubara T and Kaneyoshi T 1966 Prog. Theor. Phys. (Kyoto) 36 695-711

Moorjani K, Tanaka T and Bose S M 1971 Conduction in Low-Mobility Materials, Edited by Klein N, Tannhauser D S and Pollak M (Taylor and Francis Ltd, London) 167-73

Morita T and Horiguchi T 1971 J. Math. Phys 12 986-92

Nickel B G and Krumhansl J A 1971 Phys Rev. B 4 4354-63

Schwartz L and Siggia E 1972 Phys. Rev. B5 383-96

Schwartz L and Ehrenreich E 1972 Phys. Rev. B6 2923-30

Sokoloski M M, Moorjani K, Tanaka T and Bose S M 1972 Bull. Am. Phys. Soc. 17 31

Soven P 1967 Phys. Rev. 156 809-13

Stern E A 1971 Phys. Rev. Lett. 26 1630-2

Stroud D and Ehrenreich H 1970 Phys. Rev. B2 3197-209

Tanaka T, Sokoloski M M, Moorjani K and Bose S M 1972 J. Non-Crystalline Solids 8-10 155-159

Velicky B, Kirkpatrick S and Ehrenreich H 1968 Phy. Rev. 175 747-66

Velicky B 1969 Phys. Rev. 184 614-27

Velicky B and Levin K 1970 Phys. Rev. B2 938-47

Yonezawa F and Matsubara T 1966 Prog. Theor. Phys. (Kyoto) 35 759-76

FIGURE CAPTIONS

Figure 1. The diagrammatic representation of the first four terms in Eq.(23). The dashed vertical line represents scattering from a given site denoted by a star. The horizontal line (G_o) represents the motion in the effective medium. All sites are distinct and summation over distinct sites is implied.

Figure 2. The first diagram represents the scattering from single-site clusters while the others are some of the diagrams obtained from Fig.(1) which are appropriate to scattering from two-site clusters.

Figure 3. The density of states as a function of energy for an ordered body-centered cubic lattice.

Figure 4. The density of states Vs. energy for a random $A_{0.9}B_{0.1}$ alloy; $\beta, \gamma > 1$.

Figure 5. The density of states Vs. energy for a random $A_{0.9}B_{0.1}$ alloy; $\beta, \gamma < 1$. The insert shows the density of states in the vicinity of the energy where one would expect the effects arising from the presence of B-atoms.

Figure 6. The density of states Vs. energy for a random $A_{0.6}B_{0.4}$ alloy; $\beta, \gamma > 1$.

Figure 7. The density of states Vs. energy for a random $A_{0.6}B_{0.4}$ alloy; β, $\gamma < 1$.

Figure 8. Same as for Fig. 7 but different values of β and γ.

Figure 9. The density of states Vs. energy for a random $A_{0.9}B_{0.1}$ alloy in the split-band case ($\delta > 1$). Note the break in the horizontal scale. The vertical scale on the right is for the main band while that on the left is for the "minority" band. The results of the present work are labeled TS-CPA.

Figure 10. The real part of the diagonal coherent potential σ_o over the energy range of the "minority" band. Comparison between present results (TS-CPA) and SS-CPA.

Figure 11. The imaginary part of the diagonal coherent potential σ_o over the energy range of the "minority" band. Comparison between present results (TS-CPA) and SS-CPA. Note the break in the vertical scale.

Figure 12. The real and the imaginary part of the off-diagonal coherent potential σ_1 over the energy range of the "minority" band.

Figure 13. The density of states Vs. Energy for a random $A_{0.9}B_{0.1}$ alloy in the split-band case ($\delta > 1$), including the off-diagonal randomness. Note the break in the horizontal scale. The vertical scale on the right is for the main band while that on the left is for the "minority" band.

FIGURE 1

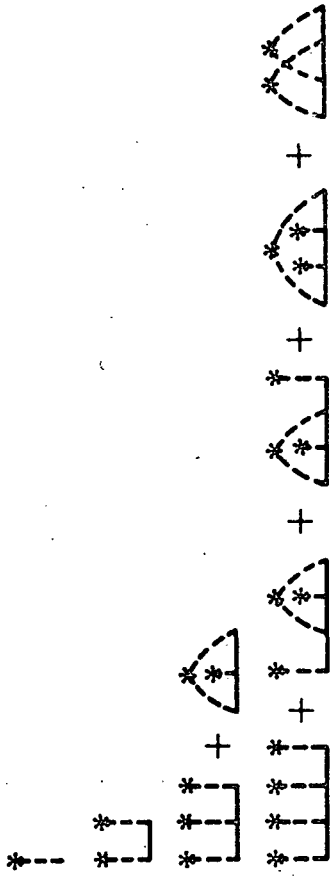

FIGURE 2

FIGURE 3

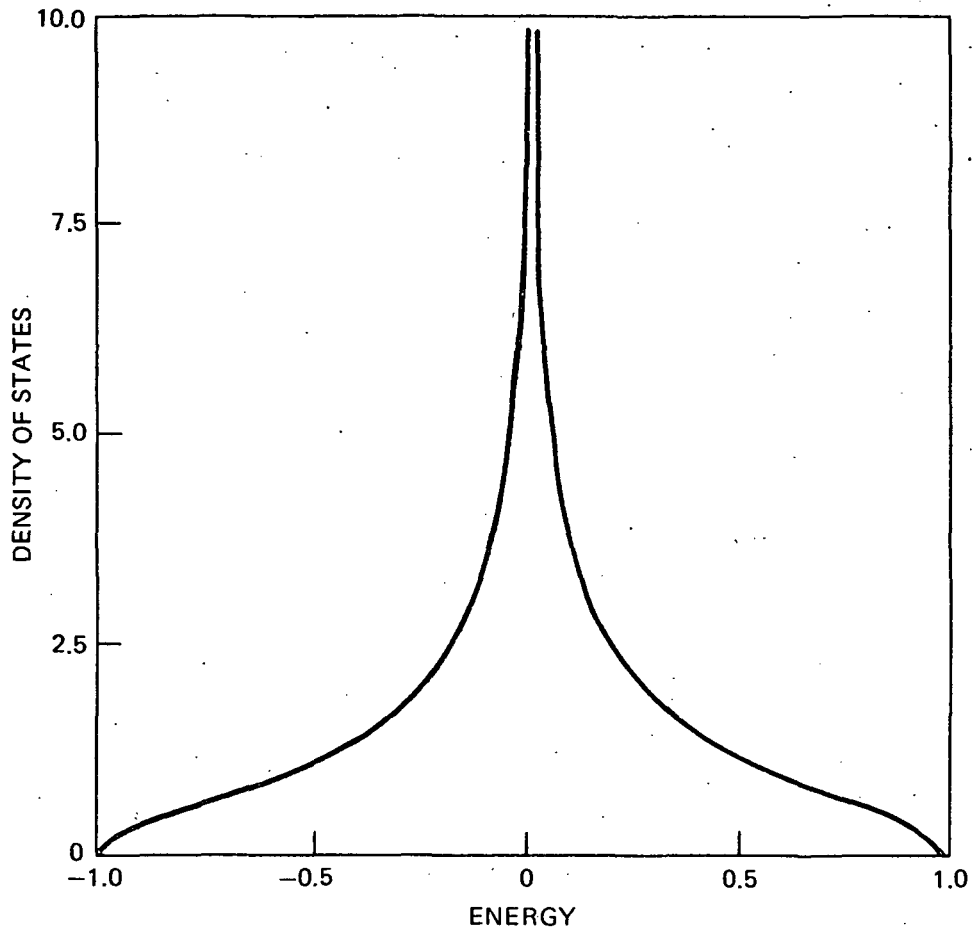

FIGURE 4

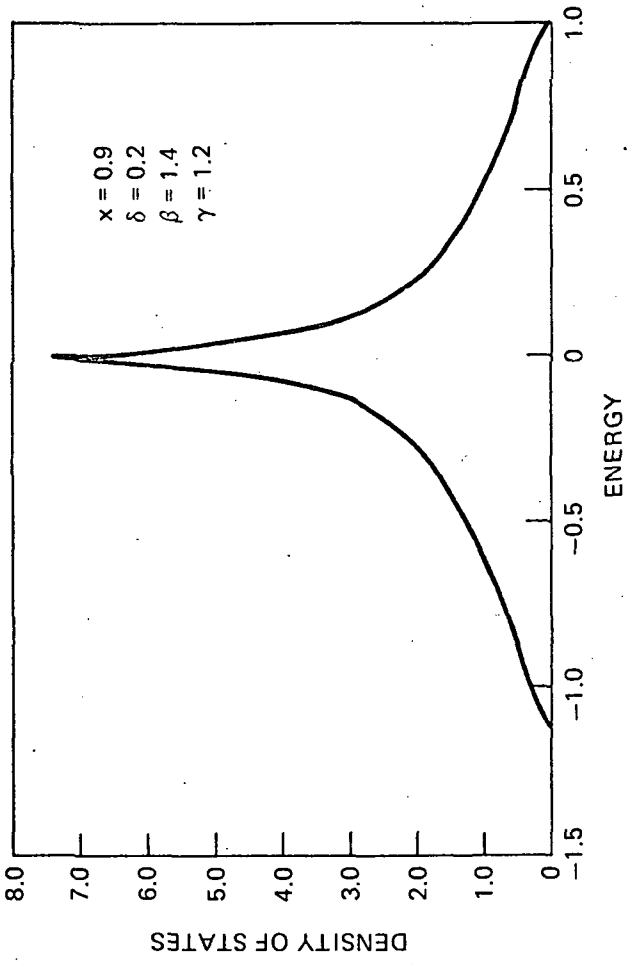
x = 0.9
δ = 0.2
β = 1.4
γ = 1.2
ENERGY
1.0
0.5
0
−0.5
−1.0
−1.5
DENSITY OF STATES
8.0
7.0
6.0
5.0
4.0
3.0
2.0
1.0
0

FIGURE 5

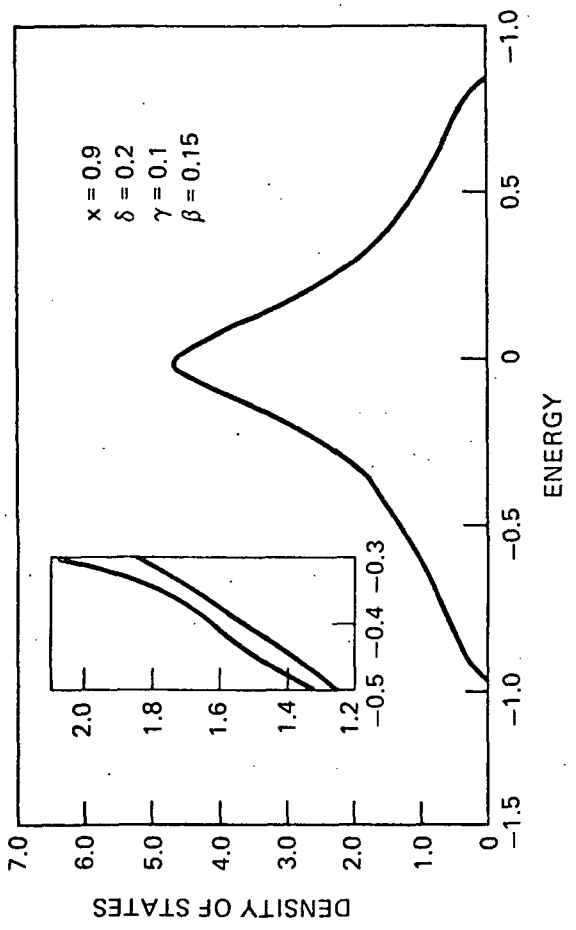
x = 0.9
δ = 0.2
γ = 0.1
β = 0.15
DENSITY OF STATES
ENERGY
7.0
6.0
5.0
4.0
3.0
2.0
1.0
0
−1.5
−1.0
−0.5
0
0.5
−1.0
2.0
1.8
1.6
1.4
1.2
−0.5
−0.4
−0.3

FIGURE 6

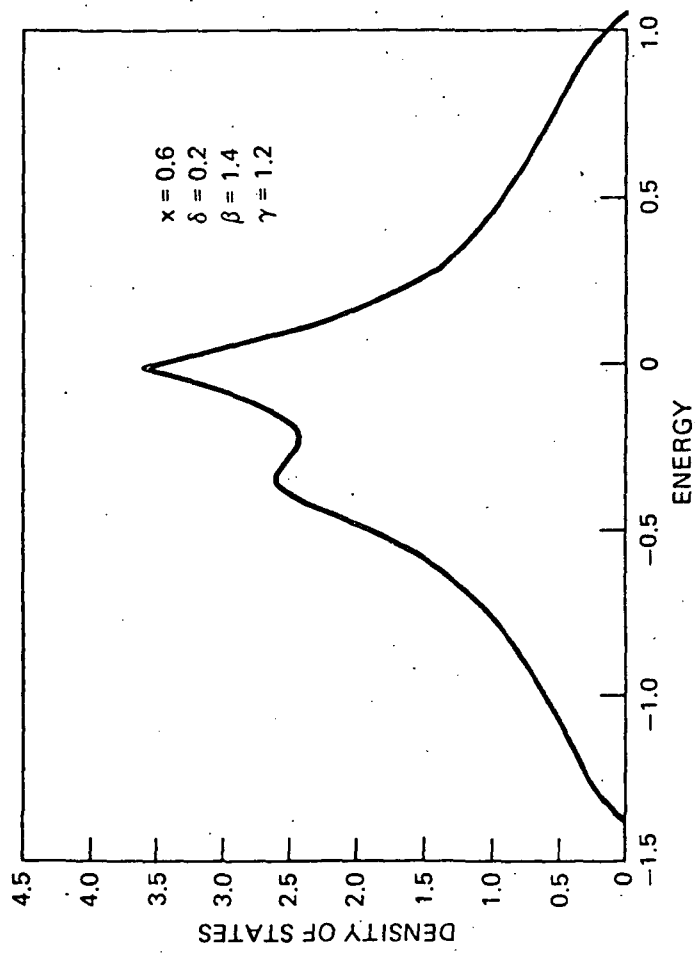
x = 0.6
δ = 0.2
β = 1.4
γ = 1.2
ENERGY
1.0
0.5
0
−0.5
−1.0
−1.5
DENSITY OF STATES
4.5
4.0
3.5
3.0
2.5
2.0
1.5
1.0
0.5
0

FIGURE 7

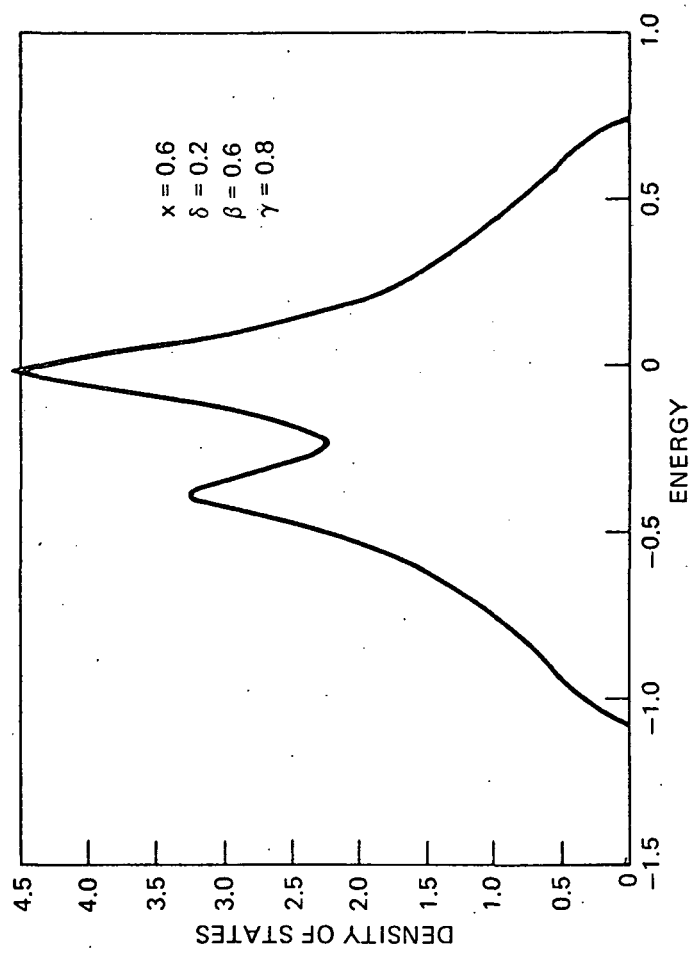
x = 0.6
δ = 0.2
β = 0.6
γ = 0.8
ENERGY
1.0
0.5
0
−0.5
−1.0
−1.5
DENSITY OF STATES
4.5
4.0
3.5
3.0
2.5
2.0
1.5
1.0
0.5
0

FIGURE 8

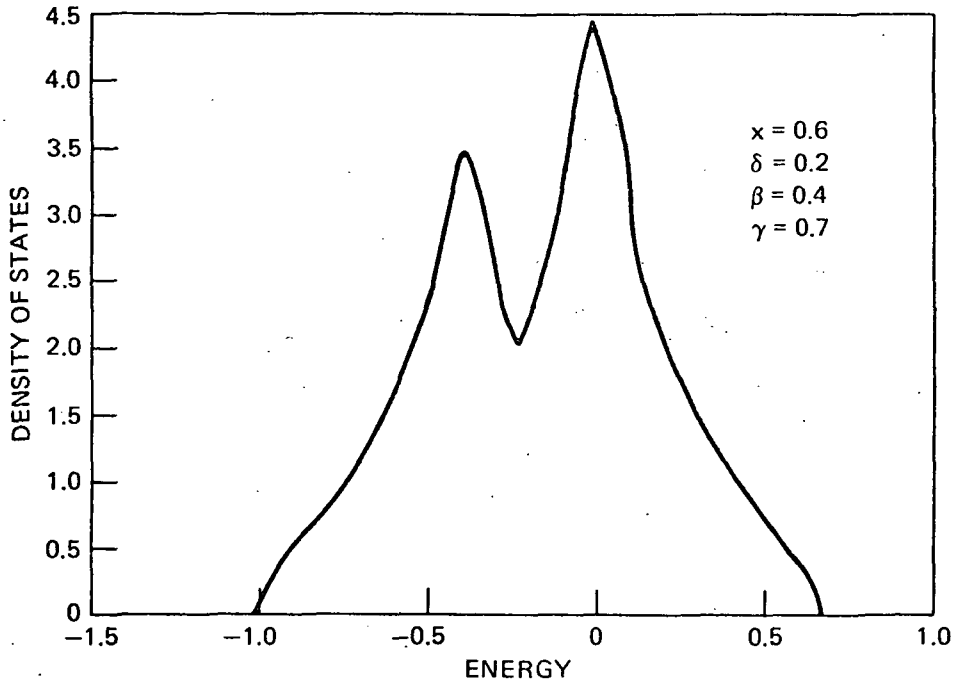
DENSITY OF STATES
4.5
4.0
3.5
3.0
2.5
2.0
1.5
1.0
0.5
0
−1.5
−1.0
−0.5
0
0.5
1.0
ENERGY
x = 0.6
δ = 0.2
β = 0.4
γ = 0.7

FIGURE 9

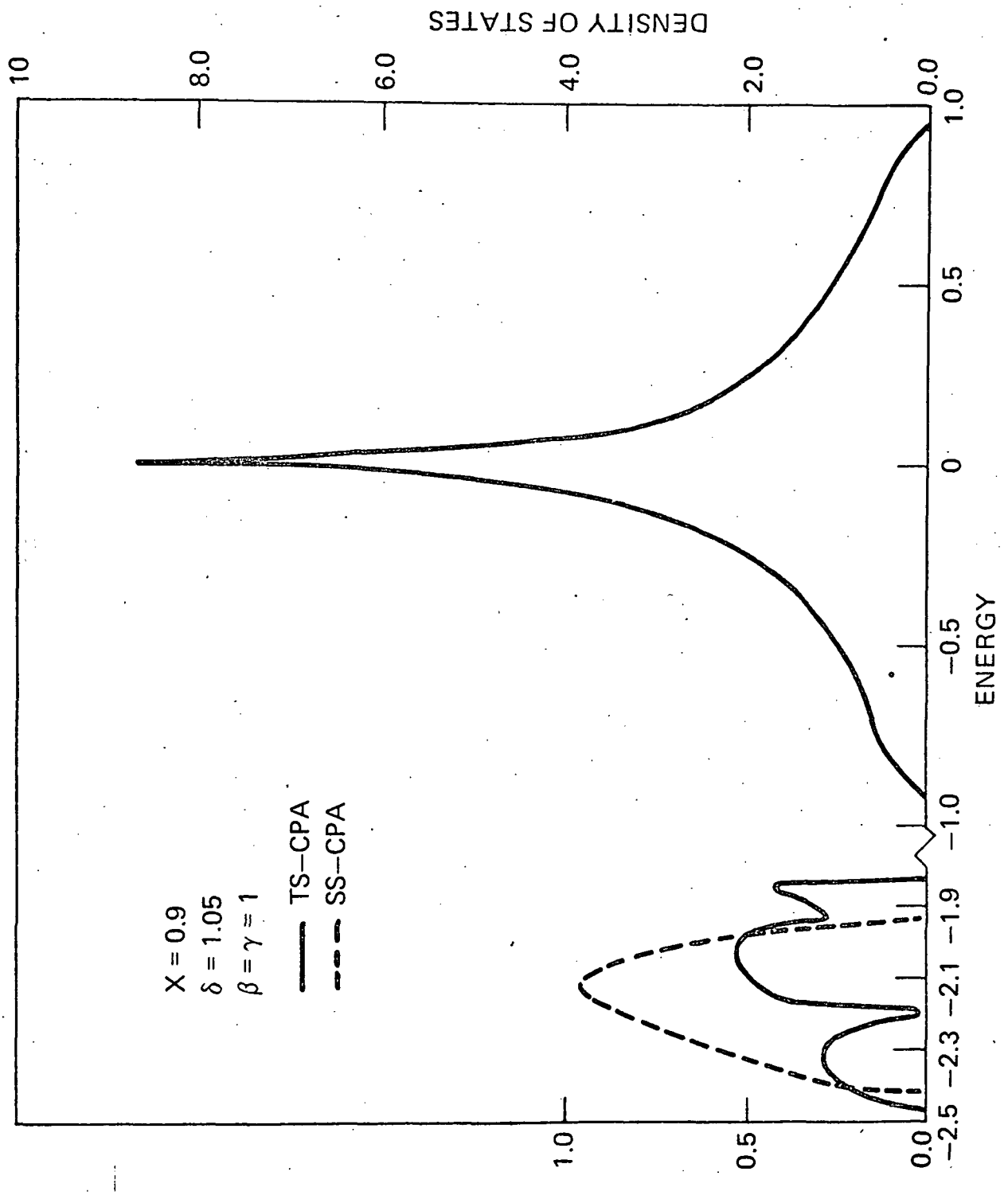
DENSITY OF STATES
10
8.0
6.0
4.0
2.0
0.0
1.0
0.5
0
−0.5
−1.0
−1.9
−2.1
−2.3
−2.5
ENERGY
X = 0.9
δ = 1.05
β = γ = 1
TS–CPA
SS–CPA

FIGURE 10

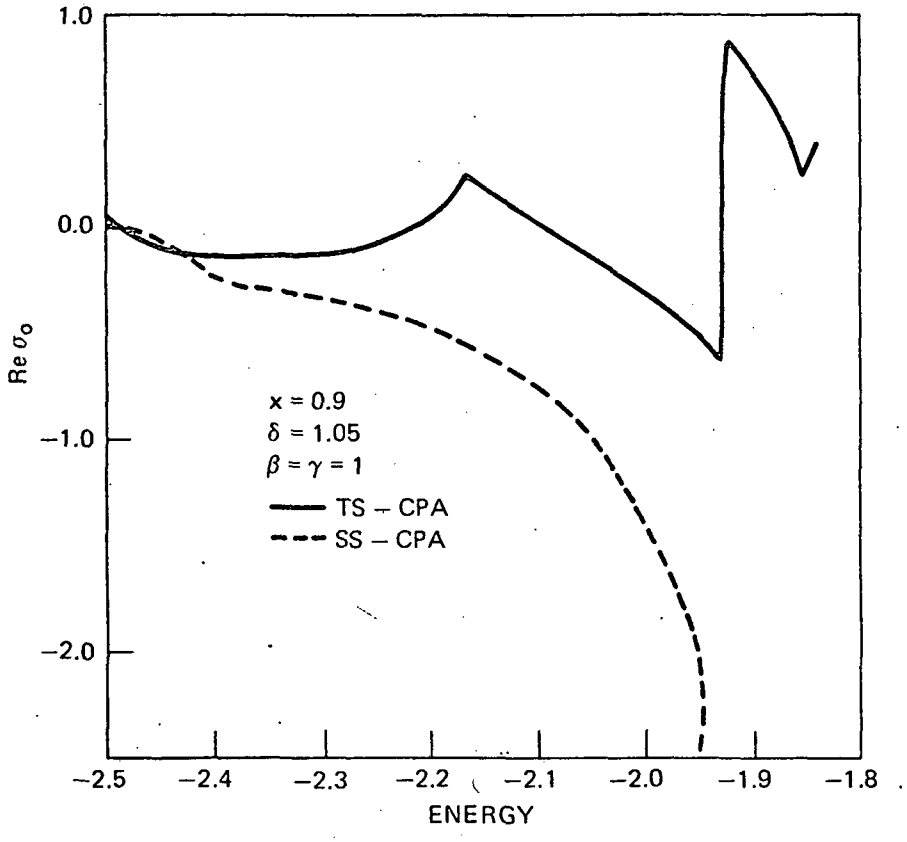
1.0
0.0
−1.0
−2.0
Re σ_o
x = 0.9
δ = 1.05
$\beta = \gamma = 1$
TS – CPA
SS – CPA
−2.5
−2.4
−2.3
−2.2
−2.1
−2.0
−1.9
−1.8
ENERGY

FIGURE 11

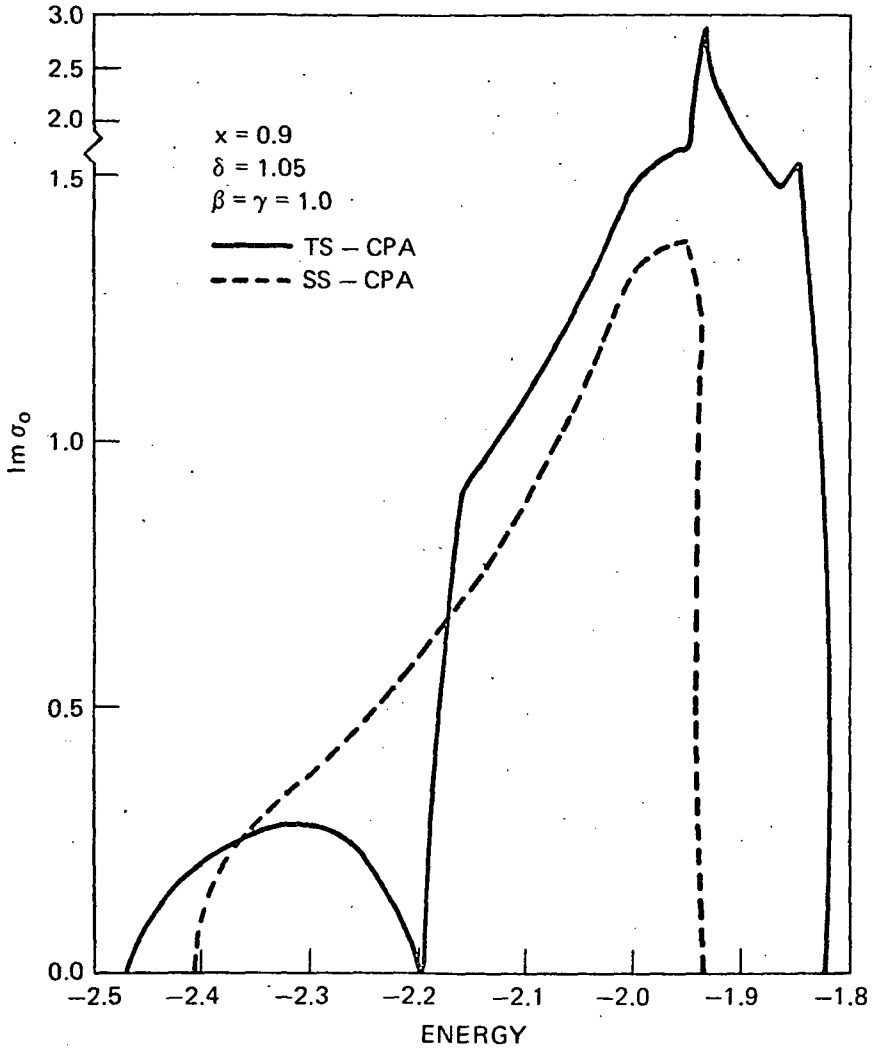
3.0
2.5
2.0
1.5
1.0
0.5
0.0
Im σ_o
x = 0.9
δ = 1.05
$\beta = \gamma$ = 1.0
TS – CPA
SS – CPA
−2.5
−2.4
−2.3
−2.2
−2.1
−2.0
−1.9
−1.8
ENERGY

FIGURE 12

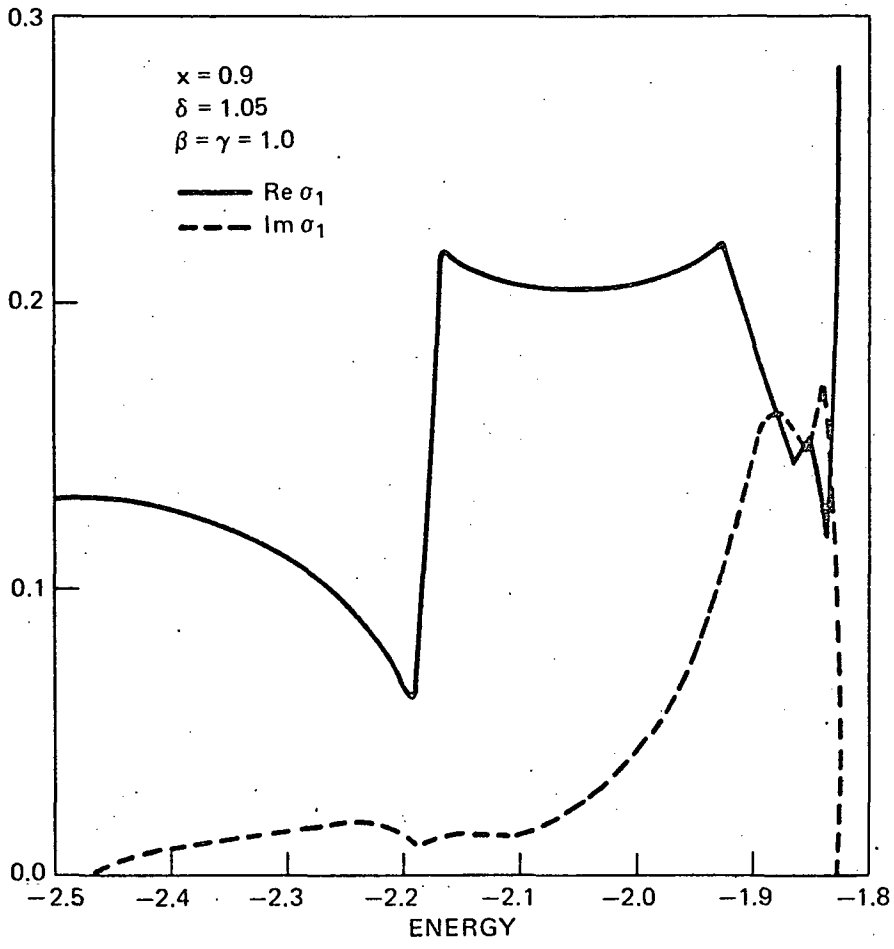

FIGURE 13

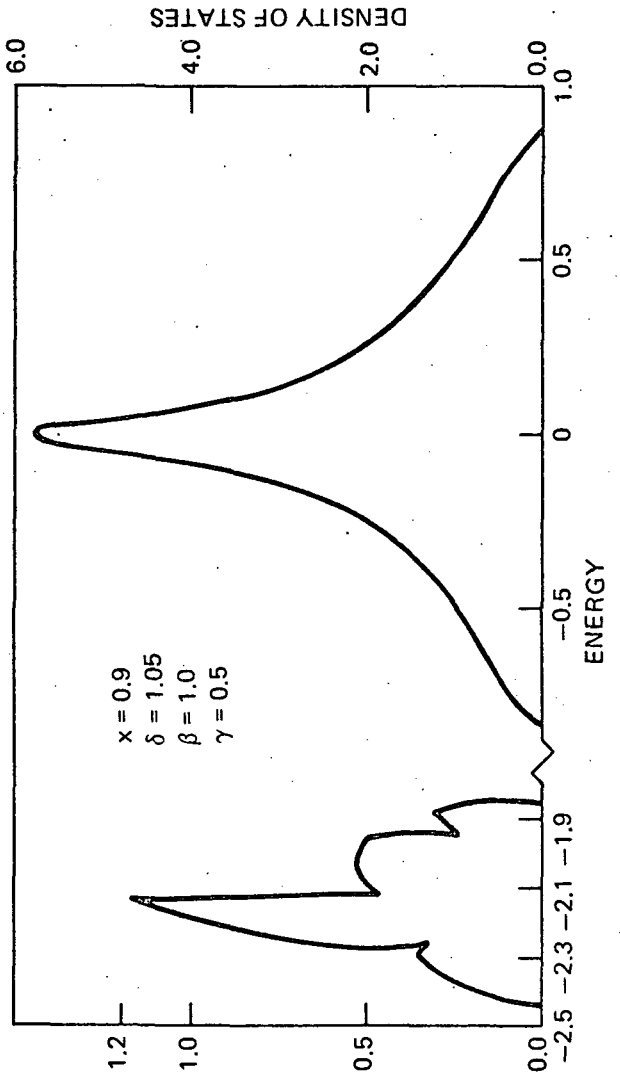
DENSITY OF STATES
6.0
4.0
2.0
0.0
1.0
0.5
0
−0.5
ENERGY
−1.9
−2.1
−2.3
−2.5
1.2
1.0
0.5
0.0
x = 0.9
δ = 1.05
β = 1.0
γ = 0.5